**Dipomarbeit**

# Building a superlattice for ultracold $^{87}$Rb-atoms

zur Erlangung des akademischen Grades
eines Magisters der Naturwissenschaften
vorgelegt von

Christian Neustetter

Institut für Experimentalphysik
an der Fakultät für Informatik, Mathematik und Physik
der Leopold-Franzens-Universität Innsbruck

November 2007

# Contents

**1 Introduction** **5**

**2 Second-harmonic generation: Theory** **10**

2.1 Nonlinear polarization density . . . . . 10

2.2 Nonlinear wave equation . . . . . 11

2.2.1 Low conversion approximation . . . . . 14

2.2.2 High conversion approximation . . . . . 18

2.3 The quasi-isotropic lithium niobate crystal . . . . . 19

2.4 Experimental methods for SHG . . . . . 21

2.4.1 QPM with periodically modulated nonlinear media . . 21

2.5 Optical properties of lithium niobate . . . . . 24

**3 Experimental part** **33**

3.1 Setup of the single-pass SHG arrangement with PPLN . . . . 33

3.1.1 A brief description of the PPLN-clip . . . . . 34

3.1.2 The home-built fiber-amplifier . . . . . 38

3.1.3 Characteristics of the oven for heating the PPLN-clip . 42

3.2 Measured dependences of SHG with PPLN . . . . . 46

3.2.1 Optimized polarization of the fundamental light . . . . 46

3.2.2 Optimum focusing for high conversion . . . . . 50

3.2.3 Dependence of QPM on the crystal temperature for different powers of fundamental light. An evidence of GRIIRA. . . . . 59

3.2.4 Harmonic power as function of fundamental power . . . 71

**4 Towards the 1D optical superlattice** **77**
4.1 Preparation of the lattice beams . . . . . 77
4.2 Stability of the superlattice . . . . . 79

**5 Summary and Outlook** **87**

**Bibliography** **92**

# Chapter 1

# Introduction

Experiments with optical lattices in Bose-Einstein condensates (BEC) and ultracold atoms have already been credited with remarkable achievements. The progressively improving control and the still increasing number of controllable parameters of these quantum systems guarantee also for the future opportunities to gain important knowledge not only of the fundamental concepts of quantum mechanics but also of new experimental applications.
Optical lattices for ultracold atoms are implemented by superimposing counter-propagating laser beams. By the resulting periodic intensity modulation of the laser light the atoms experience due to the induced dipole force a periodic potential.
The physics of ultracold atoms in optical lattices is reminiscent of the physics of crystaline structures in solid state physics. For example, the appearance of so called Bloch-oscillations, which are predicted for periodic potentials and which are hard to measure in real crystals because of various disturbing mechanisms, could already be verified by the use of ultracold atoms in optical lattices [1].
Another achievement is the controllable quantum phase transition of a BEC in an optical lattice from the suprafluid (SF) phase into the Mott-insulator (MI) phase [2, 3]. In the SF phase the wavefunction has a definite phase and is spread over many lattice sites, the local atom number of each lattice site is not well defined. The Mott phase has well defined site occupancy and

the enhanced confinement of the atoms in the same lattice site, resulting in a higher interaction between the atoms of the same site, can be used for studying strongly correlated quantum gases.
Another achievement is the coherent transfer of two Rb atoms into one $Rb_2$ molecule, which is described in [4]. Even though the so created molecules are in a high vibrational state, they show long lifetimes because they are prevented from inelastic collisions between each other by the "sheelding" of the lattice potential.
Ultracold atoms in optical lattices also have promising applications in the field of Quantum-Information-Processing (QIP). There are many proposals which utilize the properties of a MI phase of ultracold atoms in optical lattices to implement large qubit arrays for massive parallel QIP-schemes (for example see [7]).
Ultracold atoms in optical lattices thus offer a unique opportunity to study solid state physics [5, 6] and provide the necessary requirements for ultracold chemistry and QIP.
Even more advanced experiments with ultracold atoms and optical lattices are possible with so called optical superlattices. An optical superlattice is a modulated optical lattice for ultracold atoms. Various different types of optical superlattices have already been realized [8, 9, 10, 11]. For our experiment we will set up a 1D optical superlattice for $^{87}$Rb atoms with a double-well potential as the unit cell of the periodic lattice potential. Thus the 1D optical superlattice in our experiment will consist of a 3D optical lattice of wavelength $\lambda_1 = 1064$nm and an additional standing wave with a wavelength $\lambda_2 = 532$nm - that is half the wavelength of the latter - overlaid in one of the three lattice directions (see figure 1.1). As the two wavelengths are quite far from the $D_2$-line of $^{87}$Rb ( $F = 2 \rightarrow F' = 3$, 780nm) the spontaneous photon scattering rate is expected to be low, which results in a long lifetime of the ultracold atoms in the lattice potential. The parameters of the double-well potential can be controlled by varying the intensities and the relative phase of the corresponding lattice beams. So it is possible to shift the energy levels of the two wells of a double-well relative to each other and to adjust the height of the barrier between the two wells. These additional degrees of freedom

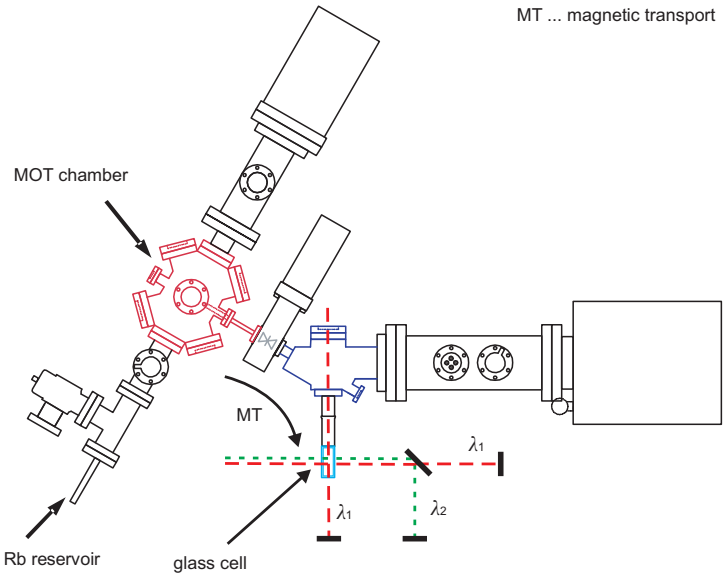


Figure 1.1: Shown is the schematic setup of the Rb-experiment and how the superlattice will be integrated in this setup (top view). The 1D optical superlattice is implemented inside the glass cell by overlaying an additional standing wave with $\lambda_2 = 0.5\lambda_1 = 532$nm in one direction to a 3D optical lattice with $\lambda_1 = 1064$nm.

for varying the shape of the unit cell potentials could be used for tunneling experiments with single atoms [9] or even molecules. Beside this, this optical superlattice utilizes the controlled transport of atoms from one lattice site to a neighbouring site, which could be used for experiments involving controlled collisions of atoms or the entanglement of atoms [13, 12, 7].

Figure 1.1 shows how the superlattice will be integrated to the existing Rb-experiment. In the Rb-experiment atoms are captured from a background rubidium ($^{87}$Rb) vapour in a magneto optical trap (MOT). After precooling the sample by an optical molasses the atoms are spin polarized and loaded into a magnetic quadrupole trap, formed by the quadrupole coils of the MOT. By using a magnetic conveyor belt [14] the cloud is then transported from the MOT chamber over approximately 40cm into the glass cell, where the atoms are loaded into a QUIC trap [15] and cooled further by evaporation. The produced BEC contains about $5 \times 10^5$ atoms. For a more detailed de-

scription of the BEC setup see [16].
For the superlattice the two lattice beams must be frequency locked. In our experiment this requirement will be accomplished by frequency doubling - which is also called second-harmonic generation (SHG)- a high power laser beam with $\lambda_1 = 1064$nm.
Within my diploma thesis I set up and characterized a single pass SHG-arrangement with periodically poled lithium niobate (PPLN) to convert a 10W laser beam with a fundamental[1] wavelength $\lambda_1 = 1064$nm into harmonic light with $\lambda_2 = 532$nm. Lithium niobate is a nonlinear optic medium with a high nonlinear electric susceptibility. Dispersion in pure lithium niobate causes a phase mismatch between the fundamental and the harmonic wave, potentially resulting in a very low conversion efficiency. A solution for reaching high conversion efficiency is to use a periodically poled lithium niobate crystal and to use quasi-phase matching (QPM) to convert fundamental infrared light efficiently into harmonic green light.
As both wavelengths of $\lambda_1 = 1064$nm and $\lambda_2 = 532$nm are quite far from the $D_2$-line of $^{87}$Rb, lattice beams with relative high powers are needed to achieve sufficient lattice depths. As the available fundamental power is limited I also had to optimize the SHG-arrangement for high conversion.
This thesis is divided into a theoretical part, an experimental part and into a part that includes considerations about the stability of the periodic double-well potential.
The theoretical part focuses on the theoretical background of the nonlinear optical effect of SHG and gives the necessary formulas used in the experimental part. In the experimental part the most important components of the SHG-arrangement are described and the dependences of SHG on the different parameters are determined and discussed. These parameters are the polarization and the focusing of the fundamental light and the crystal temperature. Beside this the dependence of the conversion for different powers

[1]During the thesis the infrared light with a wavelength of $\lambda_1 = 1064$nm will be referred to as the "fundamental" light and the frequency doubled light with a wavelength of $\lambda_2 = 532$nm will be referred to as the second-harmonic (SH) or simply the "harmonic" light. Of course, the two wavelengths are not more fundamental or more harmonic than any other wavelength.

of fundamental light is investigated. A short summary of the results of our SHG-setup and a brief outlook will conclude this thesis.

# Chapter 2

# Second-harmonic generation: Theory

In this part a brief theoretical introduction and review into nonlinear optics with focus on second-harmonic generation (SHG) is given. The main purpose is to derive the necessary formulas used in the experimental part and to provide some theoretical background. The explanations follow the textbooks [22] and [23] and are slightly modified here. An additional section is devoted to the optical properties of lithium niobate.

## 2.1 Nonlinear polarization density

A linear dielectric medium is characterized by a linear relation between the polarization density $\mathscr{P}$ and the electric field $\mathscr{E}$, $\mathscr{P} = \varepsilon_0 \chi \mathscr{E}$, where $\varepsilon_0$ is the permittivity of free space and $\chi$ is the linear electric susceptibility of the medium. A nonlinear dielectric medium, on the other hand, is characterized by a nonlinear relation between $\mathscr{P}$ and $\mathscr{E}$.
Since externally applied optical electric fields are typically small in comparison with characteristic interatomic or crystalline fields, even when focused laser light is used, the nonlinearity is usually weak. The relation between $\mathscr{P}$ and $\mathscr{E}$ is then approximately linear for small $\mathscr{E}$, deviating only slightly from linearity as $\mathscr{E}$ increases. Under this circumstances, it is possible to expand

the function that relates $\mathscr{P}$ to $\mathscr{E}$ in a taylor's series about $\mathscr{E} = 0$:

$$\mathscr{P} = \varepsilon_0 \chi \mathscr{E} + \varepsilon_0 \chi^{(2)} \mathscr{E}^2 + \varepsilon_0 \chi^{(3)} \mathscr{E}^3 + ...$$

$$= \varepsilon_0 \chi \mathscr{E} + \mathscr{P}_{NL} \tag{2.1}$$

Where $\chi$ is the linear susceptibility and $\chi^{(2)}$ and $\chi^{(3)}$ are the nonlinear susceptibilities of second and third order respectively. In the last line all nonlinear terms are combined to the nonlinear polarization density $\mathscr{P}_{NL}$. The polarization density in the medium caused by the fundamental wave can be seen as a source of electromagnetic waves, where the linear term describes linear optic effects like refraction or dispersion and the nonlinear term is responsible for the occurance of nonlinear effects like second-harmonic generation, frequency conversion, parametric amplification etc.
In the following we focus on second-harmonic generation (SHG). A more detailed explanation of other nonlinear effects can for example be found in [22] or [23].
It should be pointed out at this stage, that relation (2.1) in general is somewhat more complex than it seems here at the first sight, because for a usual medium the susceptibilities $\chi^{(i)}$ are tensors of $(i+1)^{th}$ order, which describe the anisotropic and frequency dependent properties of the medium. Fortunately, as will be explained in section 1.3, for the used setup it is sufficient to work out the theory for an isotropic medium, what simplifies the following calculations a lot.

## 2.2 Nonlinear wave equation

From Maxwell's equations for a dielectric medium a nonlinear wave equation can be derived [22]. This is the starting point for the further calculations and this differential equation will be solved here by a coupled wave theory.
Thus wave propagation in an isotropic nonlinear medium is governed by the basic wave equation

$$\nabla^2 \mathscr{E} - \frac{1}{c_\nu^2} \frac{\partial^2 \mathscr{E}}{\partial t^2} = -\mathscr{S} \tag{2.2}$$

where $\mathscr{E}$ is the electric field, $c_\nu$ denotes the phase velocity of a propagating wave with frequency $\nu$- thus describing dispersion of the medium - and where

$$\mathscr{S} = -\mu_0 \frac{\partial^2 \mathscr{P}_{NL}}{\partial t^2} \tag{2.3}$$

is regarded as a radiation source. For a second-order nonlinear medium

$$\mathscr{P}_{NL} = \varepsilon_0 \chi^{(2)} \mathscr{E}^2 \tag{2.4}$$

is the nonlinear component of the polarization density. Note that the effects of the linear susceptibility are taken formally into account by the frequency dependence of $c_\nu$ (see [22]).
As an ansatz for the solution of the differential equation 2.2 for the field $\mathscr{E}(t)$ we assume a superposition of two waves of the fundamental frequency $\nu_1$ and the second-harmonic frequency $\nu_2 = 2\nu_1$ with complex amplitudes $E_1$ and $E_2$ respectively,

$$\begin{aligned}\mathscr{E}(t) &= \sum_{q=1,2} \mathrm{Re}\left[E_q \exp(j2\pi\nu_q t)\right] \\ &= \sum_{q=1,2} \frac{1}{2}\left[E_q \exp(j2\pi\nu_q t) + E_q^* \exp(-j2\pi\nu_q t)\right] \\ &= \sum_{q=\pm1,\pm2} \frac{1}{2} E_q \exp(j2\pi\nu_q t)\end{aligned}$$

where $\nu_{-q} = -\nu_q$ and $E_{-q} = E_q^*$. The corresponding nonlinear polarization density from equation 2.4 is then given by

$$\mathscr{P}_{NL}(t) = \frac{1}{4}\varepsilon_0 \chi^{(2)} \sum_{q,r=\pm1,\pm2} E_q E_r \exp\left[j2\pi(\nu_q + \nu_r)t\right]$$

and the corresponding radiation source 2.3 is calculated to

$$\mathscr{S} = \frac{1}{4}\mu_0 \varepsilon_0 \chi^{(2)} \sum_{q,r=\pm1,\pm2} 4\pi^2(\nu_q + \nu_r)^2 E_q E_r \exp\left[j2\pi(\nu_q + \nu_r)t\right]$$

which is the sum of harmonic components $\exp[j2\pi(\nu_q + \nu_r)t]$ of frequencies that are sums and differences of the original frequencies $\nu_1$ and $\nu_2$. Substituting all into the wave equation 2.2, we obtain a single differential equation with many terms, each of which is a harmonic function of some frequency. We can separate this equation into two differential equations by equating the corresponding harmonic terms on both sides of the nonlinear wave-equation at each of the frequencies $\nu_1$ and $\nu_2$, separately. The result can be written in the form of two Helmholtz equations with the sources:

$$S_1 = 4\pi^2 \mu_0 \varepsilon_0 \chi^{(2)} \nu_1^2 E_2 E_1^*$$

$$S_2 = 2\pi^2 \mu_0 \varepsilon_0 \chi^{(2)} \nu_2^2 E_1 E_1$$

So that we obtain the two coupled differential equations:

$$(\nabla^2 + k_1^2) E_1 = -4\pi^2 \mu_0 \varepsilon_0 \chi^{(2)} \nu_1^2 E_2 E_1^*$$

$$(\nabla^2 + k_2^2) E_2 = -2\pi^2 \mu_0 \varepsilon_0 \chi^{(2)} \nu_2^2 E_1 E_1 \tag{2.5}$$

This set of differential equations can be simplified when assuming that the two waves are collinear plane waves traveling in the $z$-direction with complex amplitudes $E_q = A_q \exp(-jk_q z)$, complex envelopes $A_q$, and wavenumbers $k_q = 2\pi\nu_q/c_q$, $q = 1, 2$. It is convenient to normalize the complex envelopes by defining the variables $a_q = A_q/(2\eta_q h\nu_q)^{1/2}$, where $\eta_q = \eta_0/n_q$ is the impedance of the medium, $\eta_0 = (\mu_0/\varepsilon_0)^{1/2}$ is the impedance of free space, $n_q$ is the refractive index and $h\nu_q$ is the energy of a photon of frequency $\nu_q$. Thus the spatial dependence of the propagating waves can be written as

$$E_q = (2\eta_q h\nu_q)^{1/2} a_q \exp(-jk_q z) \tag{2.6}$$

$$q = 1, 2$$

and the intensities of the two waves are $I_q = |E_q|^2 / 2\eta_q = h\nu_q |a_q|^2$. The photon flux density (photons/(s m$^2$)) associated with these waves are then

$$\Phi_q = \frac{I_q}{h\nu_q} = |a_q|^2$$

The variable $a_q$ therefore represents the complex envelope of wave $q$, scaled such that $|a_q|^2$ is the photon flux density. This scaling is convenient since the process of wave mixing must be governed by photon-number conservation. Further, as a result of the interaction between the two waves, the complex envelopes $a_q$ vary with distance $z$ so that $a_q = a_q(z)$. If the interaction is weak, the $a_q(z)$ vary slowly with $z$, so that they can be assumed approximately constant within a distance of a wavelength. This makes it possible to use the slowly varying envelope approximation. Using this with the ansatz 2.6 the above system of coupled differential equations 2.5 can be simplified to

$$\frac{da_1}{dz} = -jg\chi^{(2)} a_2 a_1^* \exp(-j\Delta k z) \tag{2.7}$$

$$\frac{da_2}{dz} = -j\frac{g\chi^{(2)}}{2} a_1 a_1 \exp(j\Delta k z) \tag{2.8}$$

where $\Delta k := k_2 - 2k_1$ is introduced as the deviation from phase-matching and

$$g^2 = 4\pi^2 \varepsilon_0^2 \frac{\eta_0^3}{n_1^2 n_2} h\nu_1^3$$

### 2.2.1 Low conversion approximation

To study the effect of phase (or momentum) mismatch, the general equations (2.7) and (2.8) are used with $\Delta k \neq 0$. For simplicity, we limit ourselves to the weak-coupling case ($\gamma L \ll 1$ see subsection 2.2.2), which in the following chapters will be referred to as the low conversion approximation. In this case the amplitude of the fundamental wave $a_1(z)$ varies only slightly with the distance $z$, and may be assumed approximately constant. Substituting

$a_1(z) \approx a_1(0)$ in equation (2.8) and integrating we obtain

$$a_2(L) = -j\frac{g\chi^{(2)}}{2}a_1^2(0)\int_0^L \exp(j\Delta k z')dz'$$

$$= -\left(\frac{g\chi^{(2)}}{2\Delta k}\right)a_1^2(0)\left[\exp(j\Delta k L) - 1\right] \tag{2.9}$$

from which the corresponding photon-flux density of the harmonic wave

$$\Phi_2(L) = |a_2(L)|^2 = (g\chi^{(2)}/\Delta k)^2\Phi_1^2(0)\sin^2(\Delta k L/2)$$

follows, where $a_1(0)$ is assumed to be real. Consequently the intensity of the generated harmonic wave is given by

$$I_2 = \Phi_2 h\nu_2 = \frac{2\pi^2\varepsilon_0^2\eta_0^3\nu_1^2L^2}{n_1^2n_2}(\chi^{(2)})^2I_1^2(0)\left[\frac{\sin(\Delta kL/2)}{\Delta kL/2}\right]^2 \tag{2.10}$$

Note that for this result we used the model of an isotropic medium and that the fundamental and harmonic wave are plane waves.[1]
For a given phase-mismatch $\Delta k$ the $SH$-intensity

$$I_2(L) \propto \frac{\sin^2(\Delta kL/2)}{(\Delta k)^2} \tag{2.11}$$

is thus a periodic function of the interaction length $L$ with maximas of equal height at $L = 2\pi(m+\frac{1}{2})/|\Delta k|$ (see 2.1). The period length $l_c$ of this function is also called the coherence length and can be expressed with the wave length $\lambda_1$ of the fundamental wave by

$$l_c = \frac{2\pi}{|\Delta k|} = \frac{2\pi}{|k_2 - 2k_1|} = \frac{\lambda_1}{2\,|n_2 - n_1|} = \frac{\lambda_1}{2\Delta n} \tag{2.12}$$

The first maximum is found at $L = l_c/2$, which also defines the crystal length that can effectively be used for frequency doubling, because an increasing crystal length just causes an oscillation of the SH-intensity. The maximum intensities (see equation 2.11 and figure 2.1) decrease with the square of the

[1] This will be important for section 3.2.2.

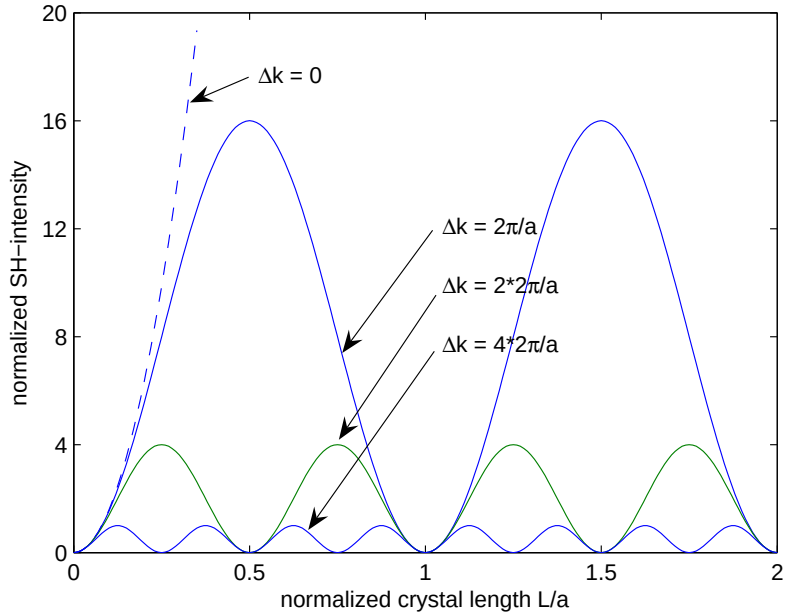


Figure 2.1: Dependence of the SH-intensity on the crystal length for different values of the phase-mismatch $|\Delta k|$. $a$ is an arbitrary scaling value. For constant $|\Delta k|$ the SH-intensity is a periodic function. The period length is given by the corresponding coherence length $l_c$ determined by equation 2.12 (see also figure 2.4).

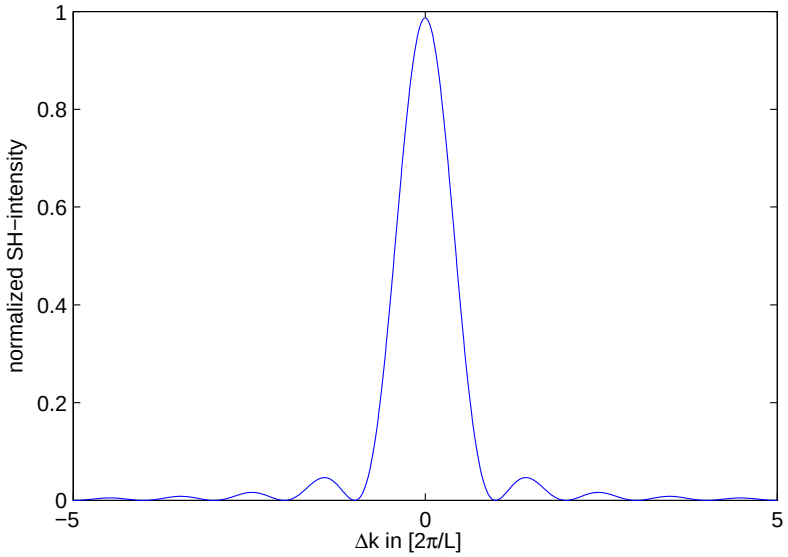


Figure 2.2: The dependence of the SH-intensity on the phase-mismatch $|\Delta k|$ for a crystal with length L. The SH-intensity has a maximum at $|\Delta k| = 0$ (perfect phase-matching) with a fullwidth of $\delta(\Delta k) := 2 * 2\pi/L$, that allows efficient SHG even when $|\Delta k| \neq 0$.

phase-mismatch $\Delta k$ and are thus proportional to $l_c^2$.
On the other hand, when the phase-mismatch $\Delta k$ is varied for a fixed crystal length, then the SH-intensity (equation 2.10) can be written as

$$I_2(L) \propto \left[\frac{\sin(\Delta k L/2)}{\Delta k L/2}\right]^2$$

This function shows a maximum with value 1 at $\Delta k = 0$ and has higher order maximas, that values decrease approximately quadratically with the order of the corresponding maximum (see figure 2.2). The intensity for the case of perfect phase-matching $\Delta k = 0$ for the low conversion approximation is given by

$$I_2 = I_1^2(0)\frac{2\pi^2\varepsilon_0^2\eta_0^3\nu_1^2L^2}{n_1^2n_2}(\chi^{(2)})^2 \tag{2.13}$$

### 2.2.2 High conversion approximation

When the conversion is high we cannot assume a fundamental wave with constant intensity along the crystal anymore. As each generated harmonic photon takes up two photons of fundamental light, pump depletion of the fundamental light in this case must be taken into account. For simplicity and to focus on the main consequences of pump depletion we assume two collinear waves with perfect phase matching ($\Delta k = 0$). Equations (2.7) and (2.8) then reduce to

$$\frac{da_1}{dz} = -jg\chi^{(2)}a_2a_1^* \tag{2.14}$$

$$\frac{da_2}{dz} = -j\frac{g\chi^{(2)}}{2}a_1a_1 \tag{2.15}$$

At the input of the crystal ($z = 0$) the amplitude of the second-harmonic wave $a_2(0) = 0$ is assumed to be zero and that of the fundamental wave $a_1(0)$ is assumed to be real. With this boundary conditions, and using the photon number conservation relation $|a_1(z)|^2 + 2|a_2(z)|^2$ =constant, equations 2.14 and 2.15 can be shown to have the solutions

$$a_1(z) = a_1(0)\text{sech}\left(\frac{g\chi^{(2)}a_1(0)z}{\sqrt{2}}\right)$$

$$a_2(z) = -\frac{j}{\sqrt{2}}a_1(0)\tanh\left(\frac{g\chi^{(2)}a_1(0)z}{\sqrt{2}}\right)$$

Consequently, the corresponding photon flux densities are given by

$$\Phi_1(z) = \Phi_1(0)\text{sech}^2\left(\frac{\gamma z}{2}\right) \tag{2.16}$$

$$\Phi_2(z) = \frac{1}{2}\Phi_1(0)\tanh^2\left(\frac{\gamma z}{2}\right) \tag{2.17}$$

where

$$\gamma^2 = 2g^2(\chi^{(2)})^2a_1^2(0) = 2g^2(\chi^{(2)})^2\Phi_1(0)$$

$$= 8\pi^2\varepsilon_0^2(\chi^{(2)})^2\frac{\eta_0^3}{n_1^2n_2}h\nu_1^3\Phi_1(0) = 8\pi^2\varepsilon_0^2(\chi^{(2)})^2\frac{\eta_0^3}{n_1^2n_2}\nu_1^2I_1(0)$$

Since $\text{sech}^2 + \tanh^2 = 1$ it follows that $\Phi_1(z) + 2\Phi_2(z) = \Phi_1(0)$ is constant, which indicates that at each position $z$, photons of the fundamental wave are converted to half as many photons of the harmonic wave. The fall of $\Phi_1(z)$ and the rise of $\Phi_2(z)$ with $z$ are shown in figure 2.3. For small $\gamma L$ - that means low conversion - the argument of the *tanh*-function is small and therefore the approximation $tanh(x) \approx x$ may be used. As a proof of consistency this yields to the same result for the harmonic intensity, that was calculated in the low conversion approximation ($a_1(z) = constant$) in subsection 2.2.1.

## 2.3 The quasi-isotropic lithium niobate crystal

Even though the calculations above were done for the special case of an isotropic nonlinear medium[2], the results can still be used for our setup with lithium niobate, which actually is an anisotropic medium concerning its refractive index as well as its nonlinear susceptibility. This simplification is possible, because in our setup the two waves propagate inside the crystal along a special direction and with a special polarization. For waves with this special propagation properties the anisotropy of the medium is of no importance and the waves propagate like in an isotopic medium: The crystal is designed for a fundamental wave propagating inside the crystal along one of its principal axis with the polarization of the fundamental light orientated parallel to the optical axis of the crystal. This fundamental light creates due to $\chi^{(2)}_{333}$ - the only relevant component of the nonlinear susceptibility in this case (see section 2.5) - a harmonic wave with the same polarization. Therefore the fundamental and the generated harmonic wave propagate inside the crystal like they would in an isotropic medium. For example the wavevector $\vec{k}$ and the Poynting-vector $\vec{S}$ of the fundamental and the harmonic wave are parallel and the direction of polarization keeps constant all through the crystal. This is in general not the case for arbitrary propagation in anisotropic

[2]For an isotropic medium tensors like the linear and the nonlinear susceptibility reduce to scalars.

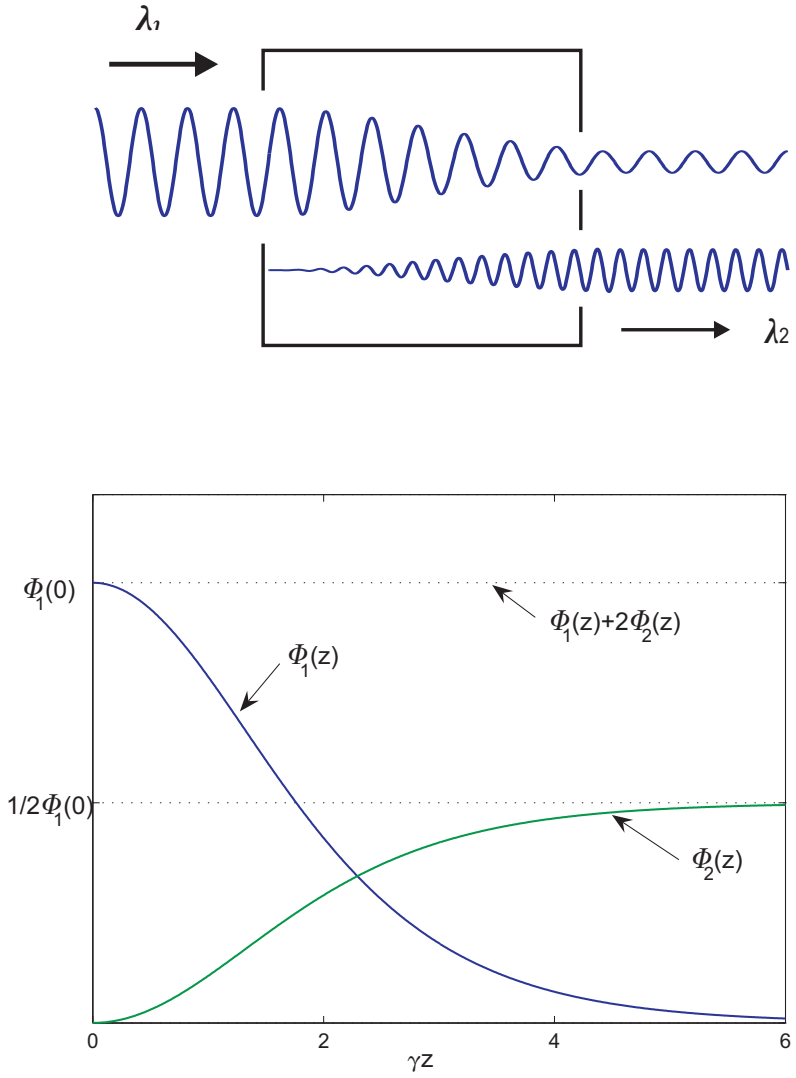


Figure 2.3: *top*: A fundamental wave with wavelength $\lambda_1$ incident on a nonlinear crystal generates a harmonic wave with wavelength $\lambda_2$. In the frequency doubling process two photons of the fundamental light combine to a photon of harmonic light, so that the increase of harmonic light goes along with the decrease of fundamental light (pump depletion). *bottom*: Shown are the corresponding photon flux densities for the fundamental and harmonic light given in equation 2.16 and 2.17. Since photon numbers are conserved, the sum $\Phi_1(z) + 2\Phi_2(z) = \Phi_1(0)$ is a constant.

media (see [22, 23]).
To summarize the theoretical results so far, we calculated the effects of phase-mismatch and the corresponding dependence of SHG on the crystal length for the low conversion limit. We also derived formulas for the generated harmonic intensity in the case of low conversion as well as for the case of high conversion, where we took pump depletion into account.
Alternatively the SHG in a photon picture can be described as a three photon process, where photon-number conservation, $\Phi_2(z) + 2\Phi_1(z) = constant$, energy conservation, $\nu_2 = 2\nu_1$, and momentum conservation, $\vec{k}_2 = 2\vec{k}_1$, hold.

## 2.4 Experimental methods for SHG

Important criteria, that should be fulfilled as well as possible for sufficient conversion, are $(i)$ phasematching of fundamental and harmonic wave - to ensure that harmonic light generated at different sites of the crystal interfere to a macroscopic harmonic wave - $(ii)$ of course a high nonlinear susceptibility $\chi^{(2)}$ and $(iii)$ - as you most often deal with beams of limited diameter - to avoid walk off of fundamental and harmonic beam. One method to achieve these requirements is to use indexmatching with birefringent nonlinear media as described in [22, 23]. Another method is to use quasi-phase matching (QPM) with periodically modulated structures, which will be explained in more detail in the following subsection.

### 2.4.1 QPM with periodically modulated nonlinear media

An alternative method to achieve efficient SHG - beside indexmatching with birefringent nonlinear media - is offered by periodically modulated structures. In principle a simple method to overcome the disturbance of dispersion would be to periodically put together regions with different dispersive dependences: Thus, what one wave gains in phase in one region relative to the other is compensated in the following region. But what is easy in principle is not necessarily easy to fabricate. A different method that is well established uses

structures with a periodically modulated nonlinear susceptibility. This is the case for the present lithium niobate crystal.

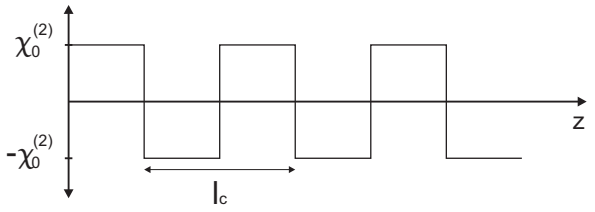


The coherence length $l_c$ determines the period length of these structures and the spatial dependence of $\chi^{(2)}$ can then be written in terms of a Fourier-series with $2\pi/l_c = \Delta k$ by

$$\chi^{(2)}(z) = \chi_0^{(2)} \sum_{m=-\infty}^{\infty} F_m e^{-j2m\pi z/l_c}$$

$$= \chi_0^{(2)} \sum_{m=-\infty}^{\infty} F_m e^{-j2m\Delta kz}$$

Where $\chi_0^{(2)}$ denotes the component of the nonlinear susceptibility relevant for the given polarization of the fundamental light (in our case this is $\chi_{333}^{(2)}$). When this is inserted into (2.8) we obtain

$$\frac{da_2}{dz} = -j\frac{g}{2}\chi_0^{(2)} \sum_{m=-\infty}^{\infty} F_m a_1 a_1 e^{(j(1-m)\Delta kz)}$$

As can be seen, the Fourier-component m=1 fulfills the phase-matching condition and leads to a linearly increasing SH-field

$$\frac{da_2}{dz} = -j\frac{g}{2}\chi_0^{(2)} F_1 a_1 a_1 \tag{2.18}$$

The other Fourier-components still are not phase-matched and cause the characteristic spatial oscillation of the SH-field (see figure 2.4). This method is called quasi-phase-matching (QPM).
In ferro-electric media like lithium niobate such structures can be implemented by producing ferro-electric domains with alternating polarity, in

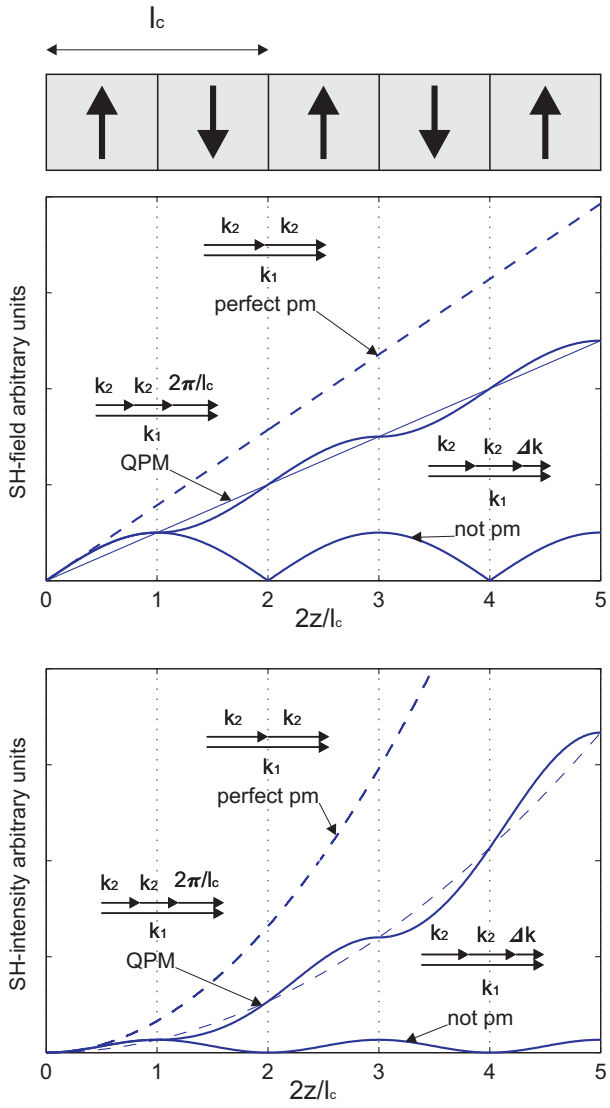


Figure 2.4: Shown is the dependence of the SH-field (*middle*) and the corresponding SH-intensity (*bottom*) on the crystal length $z$ (measured in the units of the half coherence length $l_c/2$) for the low conversion approximation and for the three different phase-matching (pm) conditions: not pm, perfect pm and QPM. (Picture taken from [23])

the way that an rectangular modulated susceptibility with period length $l_c$ is achieved. As the first Fourier-component of a rectangular function is $F_1 = 2/\pi$ the resulting SH-field obtained from equation 2.18 for the low conversion approximation is lower by a factor of $2/\pi$ and thus the SH-intensity is lower by a factor $(2/\pi)^2 \approx 0.4$ than in the case of perfect phase-matching (see equation 2.9). This decrease of conversion efficiency due to QPM is compensated by the ability to choose the direction of propagation and the polarization of the fundamental wave freely. The parameters of the fundamental wave can be chosen in the way that the highest possible component of the nonlinear susceptibility is used. Beside this, walk off can also be avoided by using the same polarization for fundamental and SH-wave or by choosing the direction of propagation in the way that both Poynting-vectors are collinear.
As already mentioned, our device is designed for a fundamental wave propagating along a principal axis of the crystal with polarization parallel to the optical axis of the lithium niobate crystal, ensuring that the Poynting-vectors of fundamental and harmonic wave are collinear and that fundamental and harmonic light have the same polarization. Fortunately the relevant component ($\chi^{(2)}_{333}$) of the nonlinear susceptibility for this polarization is the highest possible in the lithium niobate crystal (see section 2.5).

## 2.5 Optical properties of lithium niobate

In this section some of the material properties of lithium niobate will be summarized. It will be focused on the optical properties relevant for second-harmonic generation, so this is no complete discription of all properties of lithium niobate. For more information on the properties of lithium niobate see for example [33, 34, 27, 28, 29, 30].
Lithium niobate ($LiNbO_3$) is a dispersive anisotropic nonlinear crystal that faces trigonal 3m symmetry. It is a compound of niobium, lithium and oxygen. Congruent[3] Lithium niobate is artificially grown by Czochralski-

[3]They are denoted as congruent when their stoichiometry, expressed as the ratio $c_{Li}$=[Li]/([Li]+[Nb]), has a congruent composition value of 48.4%.

technique from a congruent melt of its components. Due to its wide transparency range, high electro-optic and nonlinear coefficient as well as due to its chemical and mechanical stability it is used in many applications. Some of these are frequency doubling, optical parametric oscillation, Pockels cells, Q-switches, phase and intensity modulators, wave guide substrates etc..
The transparency range of lithium niobate lies between 420nm and 5200nm and the absorption for light of the wavelength 1064nm is given by $\alpha$ =0.1%/cm [33, 34]. The propagation of light inside the crystal is governed by the linear susceptibility $\chi$. Like in all anisotropic media $\chi = \chi_{ij}$ is a tensor, that describes the directional dependence of the susceptibility. For lithium niobate at a temperature of 200°C and for light of the wavelength of $\lambda_1$ =1064nm this tensor is given by [4]

$$\chi(\lambda_1) = \begin{pmatrix} 3.99 & 0 & 0 \\ 0 & 3.99 & 0 \\ 0 & 0 & 3.69 \end{pmatrix}$$

and for light of the wavelength of $\lambda_2$ =532nm it is

$$\chi(\lambda_2) = \begin{pmatrix} 4.31 & 0 & 0 \\ 0 & 4.41 & 0 \\ 0 & 0 & 4.05 \end{pmatrix}$$

Note that the components of a tensor depend on the coordinate system you choose. In the present case a coordinate system, that diagonalizes $\chi$, was chosen. The coordinate axis of this special coordinate system are called the principal axis of the crystal. Usually components of all other tensors (eg. the nonlinear susceptibility) refer to this coordinate system too. Due to the crystal-symmetry of lithium niobate two of the three components of $\chi$ are equal $\chi_{11} = \chi_{22}$. Such crystals are termed as uniaxial crystals and the direction along the third component (in this case $\chi_{33}$) is defined as the optical axis of the crystal. The linear susceptibility is connected to the refractive

[4]The following values are calculated with the temperature dependent Sellmeier-equation on page 27.

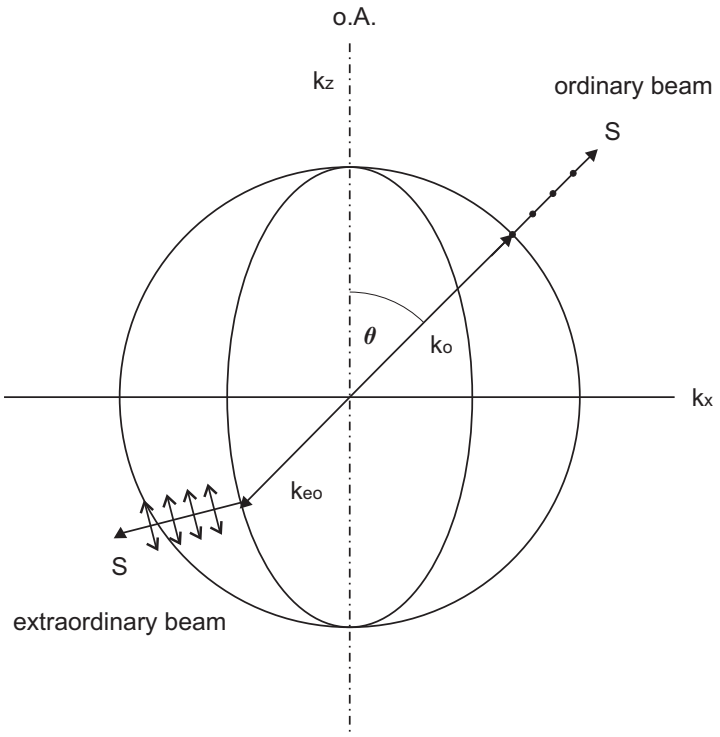


Figure 2.5: Schematic cross-section of the k-surfaces of an uniaxial medium like lithium niobate with $n_o > n_e$. The 3D k-surfaces are obtained by rotation around the optical axis (o.A.) of the crystal. The circle with radius $n_o$ indicates the isotropic refractive index for a propagating wave with its polarization perpendicular to the o.A. (ordinary wave), while the ellipse with the halfaxis $n_o$ and $n_e$ describes the directional dependence of the refractive index for an extraordinary wave. As an example $\vec{k}_o$ and $\vec{k}_{eo}$ indicate an ordinary and an extraordinary wave respectively. Also shown are the corresponding polarizations of the electric field $\vec{E}$ and the corresponding Poynting vectors $\vec{S}$. While for an ordinary wave $\vec{k}_o \parallel \vec{S}$, for an extraordinary wave $\vec{k}_{eo} \nparallel \vec{S}$, so that an ordinary and an extraordinary beam with the same direction of their wavevectors may travel in different directions (walk off).

index of the medium by the relation $n = \sqrt{1+\chi}$. Thus lithium niobate is a birefringent medium, that for a crystal temperature of 200°C and for light of the wavelength 1064nm (532nm) shows an ordinary refractive index $n_o$=2.23 ($n_o$=2.33) and an extraordinary refractive index $n_e$=2.17 ($n_e$=2.25). The refractive index, that is experienced by a propagating wave inside an anisotropic medium depends on the polarization of the wave. For each direction of the wavevector $\vec{k}$ two directions of polarization of the propagating wave can be found that allow the propagation of a linear polarized wave in the medium. These certain directions of polarization are referred to as normal modes (see [22, 23]). There always is one normal mode, that allows propagation of a wave with polarization perpendicular to the optical axis of the crystal, with its Poynting vector $\vec{S}$ in the same direction as the corresponding wavevector $\vec{k}$ and with the ordinary refractive index $n_o$. And there is another normal mode, that allows propagation of a wave with its polarization parallel to the plane spanned by the optical axis of the crystal and the wavevector $\vec{k}$. Its Poynting vector $S$ now in general deviates from the direction of the wavevector $k$ and the corresponding extraordinary refractive index $n(\theta)$ depends on the direction of the wavevector $k$. The dependence of the extraordinary refractive index is given by (see [22, 23]):

$$\frac{1}{n^2(\theta)} = \frac{\cos^2\theta}{n_o^2} + \frac{\sin^2\theta}{n_e^2}$$

Where $n_o$ and $n_e$ refer to the corresponding principal refractive indices. Beside this the refractive indices $n_o$ and $n_e$ depend on temperature. For a temperature T and a wavelength $\lambda$ the refractive indizes $n_o$ and $n_e$ can be calculated by the temperature-dependent Sellmeier-equation [34]:

$$n^2 = A_1 + \frac{A_2 + B_1 F}{\lambda^2 - (A_3 + B_2 F)^2} + B_3 F - A_4 \lambda^2 \tag{2.19}$$

Where $F = (T-24.5)(T+570.5)$, T is given in °C and $\lambda$ is given in nm. The necessary coefficients are listet in table 2.1. Also the nonlinear susceptibility $\chi^{(2)}$ of lithium niobate depends on the wavelength of the fundamental light and is anisotropic. For a fundamental wavelength of 1064nm the nonvanish-

| ***Parameter*** | $n_e$ | $n_o$ |
|---|---|---|
| $A_1$ | 4.582 | 4.9048 |
| $A_2$ | $9.921 \times 10^4$ | $1.1775 \times 10^5$ |
| $A_3$ | $2.109 \times 10^2$ | $2.1802 \times 10^2$ |
| $A_4$ | $2.194 \times 10^{-8}$ | $2.7153 \times 10^{-8}$ |
| $B_1$ | $5.2716 \times 10^{-2}$ | $2.2314 \times 10^{-2}$ |
| $B_2$ | $-4.9143 \times 10^{-5}$ | $-2.9671 \times 10^{-5}$ |
| $B_3$ | $2.2971 \times 10^{-7}$ | $2.1429 \times 10^{-8}$ |

Table 2.1: Parameters for the temperature dependent Sellmeier equation given by [34].

ing components $\chi^{(2)}_{ijk}$ of the nonlinear susceptibility $\chi^{(2)}$ - a tensor of third rank - are given by:

$$\chi^{(2)}_{222} = -\chi^{(2)}_{211} = -\chi^{(2)}_{112} = -\chi^{(2)}_{121} = 3.07\text{pm/V}$$

$$\chi^{(2)}_{311} = \chi^{(2)}_{322} = 5.95\text{pm/V}$$

$$\chi^{(2)}_{333} = 34.4\text{pm/V}$$

As already mentioned above, these components refer back to the principal axis of the crystal.

A fundamental wave propagating along a principal axis with its polarization of the fundamental electric field $\vec{\mathscr{E}} = \mathscr{E}_i$ parallel to the optical axis of the crystal ($\mathscr{E}_i = \mathscr{E}_3$) thus generates a nonlinear polarization density $\vec{\mathscr{P}_{NL}} = \mathscr{P}_{NL,i}$ also pointing parallel to the optical axis of the crystal:

$$\mathscr{P}_{NL,i} = \varepsilon_0 \chi^{(2)}_{ijk} \mathscr{E}_j \mathscr{E}_k = \chi^{(2)}_{333} \mathscr{E}_3 \mathscr{E}_3 = \mathscr{P}_{NL,3} \tag{2.20}$$

This polarization density can be seen as the source of a harmonic wave, that propagates with the extraordinary index of refraction.

An essay concerning the dependence of the nonlinear susceptibility on the fundamental wavelength can be found in [22, 23].

Beside these optical properties of lithium niobate it is worth to note that lithium niobate is a ferro-electric medium. Ferro-electric crystals are crystals

that inherently have an electric dipolmoment. In analogy to the magnetic dipol moments in a ferro-magnet the electric dipols in a ferro-electric medium orientate themselves due to their interaction into domains (see [24, 25]). In lithium niobate the electric dipol moments result from slight offsets in the position of niobium and lithium ions in the unit cell. The orientation of the crystal defines the direction of the dipol moment. On the other hand -as described in the following- it is possible to force the electric dipolmoment in a certain direction by a strong electric field and thus to orientate the crystal with its anisotropic properties. This is used for producing periodic modulated structures PPLN (Periodically Poled Lithium Niobate). PPLN is used for second-harmonic generation to achieve efficient conversion of fundamental light into harmonic light by the method of Quasi-Phase-Matching (QPM) (see subsection 2.4.1): The efficiency of frequency doubling in a dispersive nonlinear medium is limited due to dispersion. Just within the coherence length $l_c$ a macroscopic harmonic wave can build up, because after the distance $l_c/2$ the increasing phase difference between fundamental and harmonic wave causes destructive interference of the harmonic light. When at this distance the poling of the crystal is changed, the involved change of the sign of the nonlinear susceptibility causes the phase of the generated harmonic wave to jump by $\pi$, resulting in constructive interference. The phase jump induced by the change of the poling can be explained in the following way: As already mentioned the nonlinear polarization density of the medium can be seen as the source for the SH-field. The nonlinear polarization density and the nonlinear susceptibility $\chi^{(2)}$ are related by $\mathscr{P}_{NL,i} = \varepsilon_0 \chi^{(2)}_{ijk} E_j E_k$, where $E_i$ is the electric field of the fundamental wave. When $\chi^{(2)}$ changes its sign, the sign of the nonlinear polarization density also changes and thus the sign of the SH-wave, resulting effectively in a phase jump of $\pi$. By periodically poling of the crystal the SH-waves of the individual domains interfere constructively along the whole crystal, greating a macroscopic harmonic wave. As strictly speaking the fundamental and harmonic wave are not phasematched this method is called quasi-phasematching.

To fabricate PPLN the ferro-electric property of lithium niobate is utilized. As already mentioned above lithium niobate has an inherent electric dipole

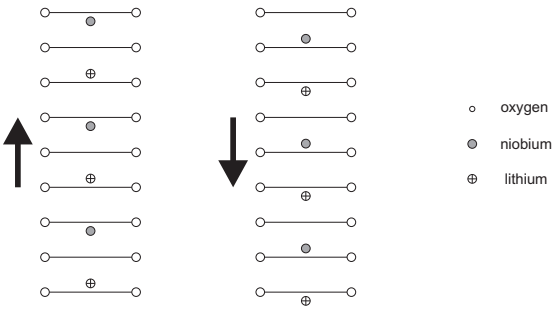


Figure 2.6: Schematic illustration of the crystal lattice of lithium niobate in both possible configurations. By applying a proper electric field one configuration can be transformed into the other and the nonlinear susceptibility changes its sign. The arrows correspond to the ones in figure 2.4. (Picture taken from [23].)

moment, to which the crystal structure is orientated. The crystal structure and thus the orientation of the anisotropic properties of the crystal can be changed by changing the direction of the poling of the crystal. When the poling is changed contrary to the previous orientation of the crystal, the metal ions change place (see figure 2.6) and the crystal ends up in a crystal, that is mirrored relative to the initial crystal by the plane perpendicular to the applied electric field. The nonlinear susceptibility for example then changes its sign. This change in sign can be explained formally by using the properties of a tensor of third rank like $\chi^{(2)}$ under a coordinate transformation $\sigma = \sigma_{ij}$ that accomplishes the mirroring:

$$\widetilde{\chi}^{(2)}_{ijk} = \chi^{(2)}_{lmn}\sigma_{li}\sigma_{mj}\sigma_{nk}$$

where the mirroring matrix is given by

$$\sigma = \begin{pmatrix} 1 & 0 & 0 \\ 0 & 1 & 0 \\ 0 & 0 & -1 \end{pmatrix}$$

For the component $\widetilde{\chi}^{(2)}_{333}$ of the crystal with changed poling this gives:

$$\widetilde{\chi}^{(2)}_{333} = \chi^{(2)}_{333}\sigma_{33}\sigma_{33}\sigma_{33} = -\chi^{(2)}_{333}$$

So changing the polarization of the crystal effects the nonlinear susceptibility to change sign.

Periodically poled structures are realized by fabricating ferro-electric domains with alternating polarity. In lithium niobate the poling is done by applying an electric field of about 20kV/mm. The length of the domains is determined by the lateral dimensions of the auxiliar electrode structure, that is used to apply the electric field. Starting point is a homogenious polarized crystal, into which a rectangular modulated susceptibility is created by a periodic electrode structure with a certain period length. More information about the fabrication of PPLN can be found in [26]. The resulting spatial dependence of the nonlinear susceptibility is rectangular and it is permanently imprinted in the crystal even when the electric field is removed.

At the end of this section two effects, that appear in lithium niobate and that are also relevant for second-harmonic generation, should be posed. These are the photo-refractive effect and an effect called Green-Induced InfraRed Absorption (GRIIRA).

The photo-refractive effect describes the change of the refractive index of a medium due to the presence of light: When a green light beam propagates through lithium niobate it has been observed, that the profile of the beam became distorted after some time [31]. This distortion is due to a change of the refractive index. The distortion is stored in the medium for several days and can be erased by illuminating the crystal completely with a constant intensity. The effect is caused by impurities of Fe-iones that enter the crystal due to imperfections during the growing of the crystal. The energy levels of these Fe-impurities lie between the valence and the conduction band of lithium niobate and their electrons can easily be excited to the conduction band. The excited electrons in the conduction band are redistributed by different transport mechanisms and cause a charge depletion modulation to build up. The electric field caused by this charge depletion modulation ef-

fects the refractive index of the medium to change via the electro-optic effect (Pockels-effect). A simplified theoretical treatment of the photo-refractive effect is given in [22] and more details can be found in [31, 32]. The photo-refractive effect can be minimized by keeping the lithium niobate crystal at elevated temperatures, because with increasing crystal temperature the mobility of of the charge carriers increases and they recombine faster, so that no charge depletion modulation can build up. Another way to prevent photo-refraction in lithium niobate and to allow working at room temperature is by doping the crystal with Mg [35].

The second effect, that is appearing in lithium niobate and that disturbs second-harmonic generation here, is Green-Induced InfraRed Absorption (GRIIRA): Due to the band gap of about 4eV in lithium niobate the absorption of infrared light from the ground state is low ($\alpha$ =0.1%/cm). But when green light is present, electrons due to Fe-impurities are excited to energy levels in-between the band gap, from where they can be excited further by absorbing infrared light. So this effect causes an additional decrease of fundamental power and thus influences the conversion efficiency of second-harmonic generation (see section 3.2.4). For more profound information about GRIIRA see for example [38]. Similar to the photo-refractive effect GRIIRA can be minimized by high crystal temperatures or by doping of lithium niobate with Mg [35].

# Chapter 3

# Experimental part

## 3.1 Setup of the single-pass SHG arrangement with PPLN

To keep things simple we set up the frequency doubling arrangement as a single pass SHG[1] system. In such a system the fundamental pump beam is focused into the nonlinear crystal and passes the medium just once. Further you do not have to build and stabilize a cavity, but to reach the high electric fields necessary for nonlinear optics, a source of sufficient high fundamental power is needed.
In this setup shown in figure 3.1 a self made fiber-amplifier[2] delivers fundamental power with wave length $\lambda_1 = 1064$nm of up to over 10W.
To align the fundamental beam high power mirrors which are highly reflective at the fundamental wavelength are used.
The low order ($\lambda/2$)-waveplate in front of the focussing lens is mounted rotateable to allow the adjustment of the polarization of the fundamental light.
A standard plano convex lens ($f = 75$mm) of Casix with an AR-coating at the fundamental wavelength focuses the fundamental beam into the crystal. The plane side of the lens is orientated to the crystal to minimize spherical aberration, although for the occurring beam diameter and waist spherical

[1] Abbreviation for second-harmonic generation, that is frequency doubling.
[2] For more details see section 3.1.2.

aberration should play a minor role.
The nonlinear medium used in this setup is lithium niobate. To get harmonic light out of the crystal Quasi-Phase-Matching (QPM) is used by periodically poling of the ferro-electric medium. Details of this method are explained in the theory part in subsection 2.4.1. To prevent the PPLN[3]-crystal from photo-refractive damage it must be kept at temperatures between 160°C and 200°C and thus it is fixed in a small oven. The oven is screwed on a mount that ensures tilting around the horizontal transverse and the vertical axis and allows limited adjustment in all three directions of space. The necessary degrees of freedom of the oven together with the crystal can so be well adjusted.
A lens behind the oven is used to (re)collimate the fundamental and harmonic beam. As there was no lens with AR coating for 1064nm and 532nm available at this time, an uncoated lens is used to keep reflection losses low.
A dielectric mirror separates the fundamental and harmonic light: 99.8% of the green light is reflected and 86% of IR light is transmitted.
For efficient SHG it is necessary to adjust the polarization and the focusing of the fundamental beam as well as the temperature of the crystal. The dependences of these parameters and measurement results will be discussed in some detail in the following subsections.
But first the necessary elements like the PPLN-clip, the fiber-amplifier and the oven will be discussed in some detail.

### 3.1.1 A brief description of the PPLN-clip

The nonlinear crystal used to convert the fundamental light with wavelength $\lambda_1 = 1064$nm into green light with wave length $\lambda_2 = 532$nm is congruently grown lithium niobate, which has a nonlinear susceptibility coefficient $\chi^{(2)}_{333} = 34.4$pm/V [33].
There are three gratings on the crystal with different poling periods (6.58$\mu$m, 6.54$\mu$m, 6.50$\mu$m), that allow frequency conversion by QPM for fundamental light of wavelength between 1059.8nm and 1067.6nm at crystal temperatures

[3]Abbreviation for periodically poled lithium niobate.

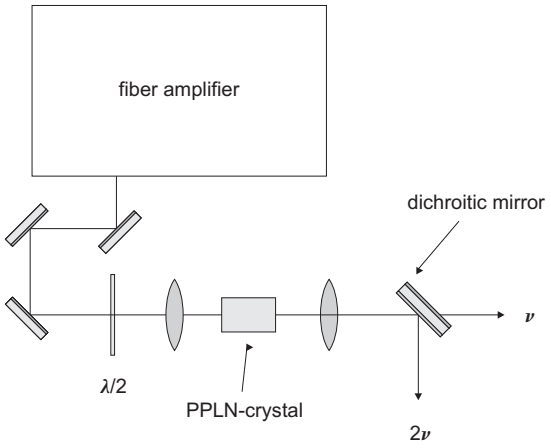


Figure 3.1: The schematic setup of the frequency doubling arrangement. It is implemented as a single-pass-configuration, simply focusing fundamental light of wave length $\lambda_1 = 1064$nm into the PPLN-crystal. Due to the nonlinear property of the medium the invisible fundamental light (IR wavelength 1064nm) is converted into bright green light of wave length $\lambda_2 = 532$nm. The method to get harmonic light out of the crystal is called Quasi-Phase-Matching (QPM).

of about 160°C, 180°C and 200°C respectively. All QPM temperatures are above 150°C which should minimize the effects of photo-refraction[4] and GRI-IRA[5] inside the crystal.

Stratophase produces the periodically poling by depositing periodic electrode structures lithographically on a lithium niobate wafer. Then for some milliseconds a voltage is applied that generates a very large electric field of about 22kV/mm. Due to the ferro-electric property of lithium niobate the applied electric field periodically inverts the crystal structure and thus the nonlinear susceptibility of the crystal (see section 2.5). The periodic structure is permanently imprinted into the crystal, because for flipping of a domain a lot of energy would be needed. By careful control of the applied voltage they achieve with this method that the fraction of periods that are merged or missing is lower than 5%. The grating next to the saw cut reference mark

[4]For a brief description of the photo-refractive effect see section 2.5.

[5]Abbreviation for Green-Induced InfraRed Absorption, see section 2.5.

has the largest poling period.
Each grating is 0.5 mm wide, 20 mm long and is separated by the neighbouring one by 0.2 mm.
The crystal itself is 10mm wide 0.5 mm thick and 20 mm long. Its input and output facets are perpendicular to the gratings within $\pm 0.15°$ and the parallelism between the facets is within $\pm 5'$.
The high refractive index of lithium niobate (n>2)[6] causes a high reflectivity when light enters or leaves the crystal. For light incident perpendicular on the crystal facet the reflectivity is estimated to:

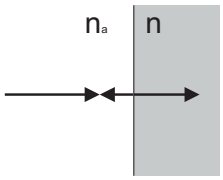


$$R = \left(\frac{n_a - n}{n_a + n}\right)^2 \approx \left(\frac{1-2}{1+2}\right)^2 \approx 10\% \tag{3.1}$$

$n_a \approx 1$... refractive index of air
$n \approx 2$... refractive index of lithium niobate

Therefore to minimize reflection losses, the two facets are AR-coated:
The input facet has a rest reflectivity of less than 0.5% for the fundamental input wavelength of 1064 nm and the output facet has a rest reflectivity of less than 0.5% at the converted wavelength of 532nm, whereas for the fundamental wavelength of 1064nm the output facet shows quite a high reflectivity of 20%.
Lithium niobate is an anisotropic medium in which the refractive index as well as the nonlinear susceptibility depend on the direction of the wavevector $\vec{k}$ and the polarization of the electric field $\vec{E}$ of a propagating wave in the

[6] As already mentioned in section 2.5 for the wavelength of 1064nm the ordinary index is $n_o = 2.23$ and the extraordinary index is $n_e = 2.17$.

medium. The coefficients of the tensors $n_{ij}$ and $\chi^{(2)}_{ijk}$ apply to the principal axis of the crystal. For calculations in an uniaxial crystal like lithium niobate it is sufficient to know the orientation of the optical axis of the crystal. The optical axis of the crystal is orientated as shown in figure 3.2.

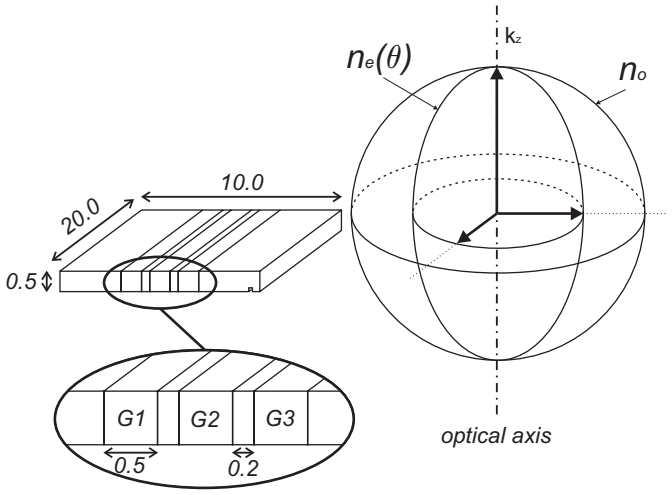


Figure 3.2: The lithium niobate crystal is about 20 mm long, 10 mm wide and 0.5 mm thick. The fundamental beam must be focused along one of the three gratings in the middle of the crystal, so that the fundamental wave propagates along a principal axis of the crystal with its polarization parallel to the optical axis of the crystal. Thus the fundamental wave propagates as an extraordinary wave. The schematic k-surfaces for ordenary and extraordenary propagation and the principal axis are orientated as shown in the figure. For a negative uniaxial crystal like lithium niobate $n_o > n_e$.

To achieve high conversion it is necessary to work at high intensities of fundamental light. But the intensity should not exceed the damage threshold of the crystal given by 0.5 MW/cm$^2$ or higher.
To avoid crystal damage it should not be heated or cooled faster than 10°C/min and the crystal temperature should not exceed 220 °C.
To ease the handling of the crystal it is mounted on a clip that consists of an alignment body, a glass-window and retaining springs, which press the two parts together.
It is important to keep the facets clean and that the adjustment of the crys-

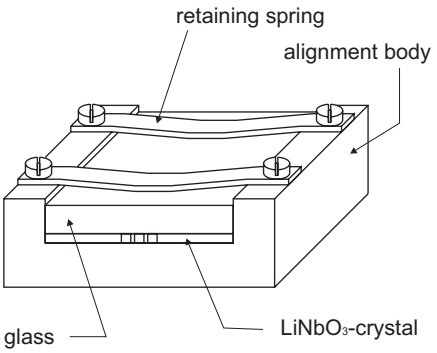


Figure 3.3: The crystal is mounted on a clip that consists of the alignment body, a glass-window, the lithium niobate crystal and retaining springs.

tal is done just with low fundamental power (we used some 10 mW) because local heating of the crystal due to dust or deadjustment of the fundamental beam at high powers can result in crystal damage.

### 3.1.2 The home-built fiber-amplifier

This chapter serves to briefly explain the functional principle of the fiber-amplifier, which delivers the fundamental power necessary for the frequency-doubling arrangement. Beside this the most relevant components are described and the characteristics of the amplified output beam will be given. This home-built[7] fiber-amplifier utilizes an amplification of 1064nm 0.5W narrow line width seed-light up to an output power of over 10W of linear polarized light single mode with a $TEM_{00}$ Gaussian mode and with a long term power stability of 0.4%/h at the output power level of 10W. The spectral linewidth and the frequency stability of the amplified output light is determined by the properties of the seed light. The schematic setup of the fiber-amplifier is shown in figure 3.4. The heart of the amplifier is the active fiber, in which the seed-light is amplified. This fiber (PLMA-YDF-20/400) was fabricated by Nufern. The specification means that it is a Polarization-Maintaining Large-Mode-Area Ytterbium-Doped Double-Clad fiber.

[7]Our fiber-amplifier was designed by H.C. Nägerl and built by M. Theis and F. Lang. For further details see [39].

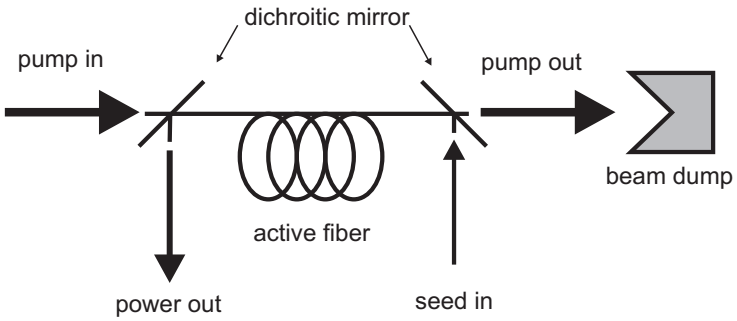


Figure 3.4: Simplified schematic setup of the fiber-amplifier. The seed and the pump light propagate in opposite directions. the advantage of this is, that there is no pump light at the output. The coiling of the active fiber is used to suppress higher order modes, so that the amplified light leaves the fiber single mode with Gaussian beam profile. To yield 10W of amplified light about 0.5W of seed light and about 25W of pumping light are used.

The doping of the fiber core with the rare earth element Ytterbium is good for amplification of light with a wavelength of about 1$\mu$m. There are also active fibers available with other dopants like Erbium, Thulium etc, that allow amplification of other wavelengths.
The increased mode field diameter of Large-Mode-Area (LMA) fibers (core/cladding: 20$\mu$m/400$\mu$m) compared to the dimensions of standard fibers (core/cladding: 10$\mu$m/125$\mu$m) is useful for generating high cw powers because detrimental effects of various nonlinear interactions such as stimulated Brillouin scattering (SBS) are reduced.
While the cladding acts as a waveguide for the pump light the core is the active region, where the pump light is absorbed by the rare earth ions. Due to the resulting population inversion lasing occurs in the core. The core also defines the transverse modal structure and the resulting beam quality of the amplified light.
The fiber used in our amplifier has a length of about 5m and reaches an amplification per meter of about 4/m (also see figure 3.6). The polarization maintaining property of the fiber ensures that the amplified light is linearly polarized. The seed light of wavelength 1064nm is delivered by the ultra-

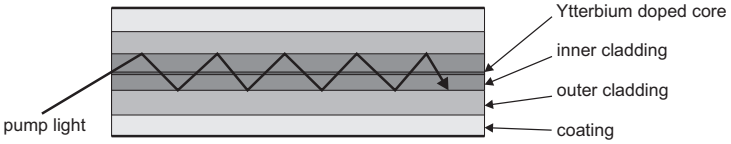


Figure 3.5: Schematic design of the active fiber. The pump light is absorbed by the rare earth ions in the core and is converted into laser light. The double clad structure acts as a wave guide for the pump light.

stable cw single-frequency Mephisto from Innolight. The properties of the seed light concerning its spectral linewidth (1kHz/100ms) and its frequency stability (1MHz/min) determine the corresponding properties of the amplified light at the output of the amplifier.

As the source for the pump light with a wavelength of about 980nm (shorter than the wavelength of the seed light ) a high-power diode laser from Jenoptics is used. It must be temperature controlled to guarantee a stable operation concerning its output power and wavelength. The pump power can be tuned easily by tuning the current of the power supply of the laser stack. For our amplifier configuration a pump power of up to 25W is used. A home-built controller-box regulates and monitors the relevant parameters of the fiber-amplifier. It regulates the temperature of the pumping laser as well as it monitors the presence of the necessary power level of the seed light. If the latter is to low, the pumping laser is switched off for safety reasons, because running the amplifier at high pumping powers when not enough seed light - that clears away the absorbed energy - is present would cause a damage of the fiber. As the fiber-amplifier arrangement is designed for a seed light of about 0.5W, the controller-box also switches off when the pump power exceeds 25W.

When the amplifier was tested for the first time, oscillations of the output power were observed always before the fiber got damaged. Thus an additional protection was implemented, that causes the pumping laser to switch off whenever an oscillation of the output light occurs. Thus at the one hand the fiber was not damaged anymore, but on the other hand the protection is

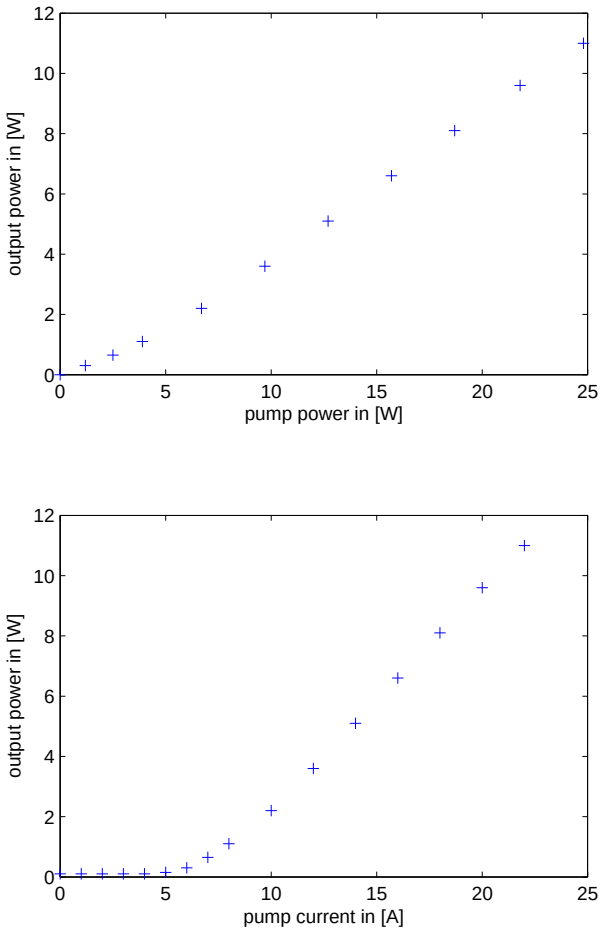


Figure 3.6: Shown are the dependences of the output power of the amplified light on the power of the pumping light (*top*) and on the current of the power supply of the pumping laser (*bottom*). The power of the seed light is about 0.5W. For pump powers and currents larger than the corresponding threshold of 2W and 5A respectively the output power increases approximately linearly with the slopes of 0.48W/W and 0.73/A respectively.

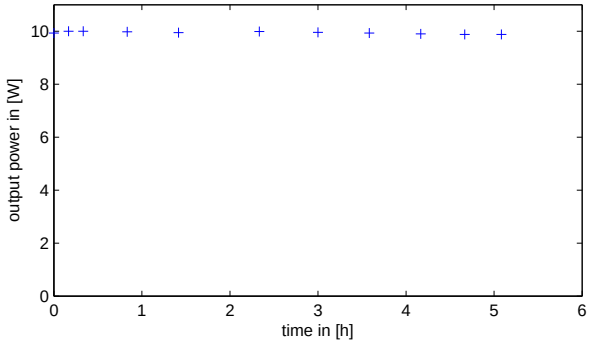


Figure 3.7: The long term stability of the output power of the fiber-amplifier shows a slight decrease of 0.4%/h.

sensitive enough to cause the amplifier to switch off when mechanical vibrations occur (for example when putting some optics on the table in the vicinity of the amplifier). The dependence of the output power of the amplifier on the pump power and on the current of the power supply of the pumping laser is plotted in figure 3.6, whereas the long term stability at an output power of 10W is shown in figure 3.7. The amplifier delivers linear polarized light, single mode with a $TEM_{00}$ Gaussian beam profile.

### 3.1.3 Characteristics of the oven for heating the PPLN-clip

To minimise photo-refractive damage of the crystal and to reduce the effect of Green-Induced-InfraRed Absorption (GRIIRA) Stratophase recommends keeping the crystal at temperatures above 160°C. To achieve efficient quasi-phase-matching it is necessary to tune and regulate the temperature.
Therefore the crystal must be kept in an oven, which is designed for use of the PPLN-clip of Stratophase and is a commercially available product.
The clip is fixed in the oven above the heating element by retaining bolts and can be removed and replaced easily. As the PPLN-clip is merely pressed onto the heating plate, thermal contact between heating plate and clip seems

not to be good.
In the oven there is a 12-24V 3.6-15W heating element, that allows to heat the crystal to temperatures ranging from ambient room temperature up to about 200°C. A PT100 resistance is used to measure the temperature. It is glued on the socket of the oven's heating plate. The drawback of this is that the PT100 is quite far away from the crystal and as the thermal contact between PPLN-clip and heating plate seems not to be good, it is thus not the actual temperature of the crystal that is measured and regulated. This gets crucial when high powers are involved (see section 3.2.3).
The oven is insulated, so that even when it is operated at 200°C the outside of the oven can easily be handled without any precaution. Small slits at the front and the back of the oven's thermal isolation allow the fundamental and harmonic beam to pass.
To adjust the PPLN clip relative to the fundamental input beam the whole

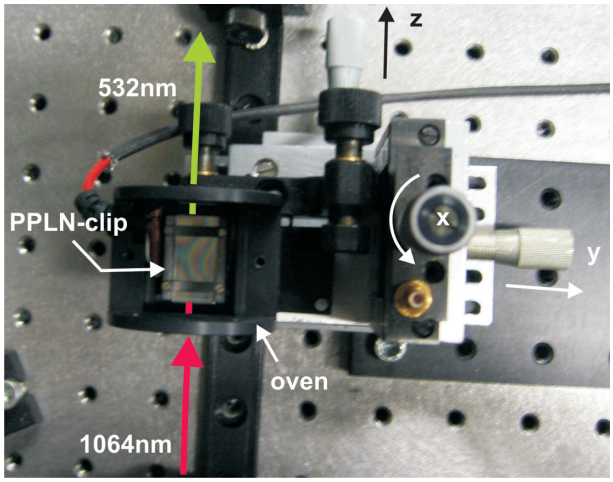


Figure 3.8: The oven is screwed on a mirror mount for tilting the crystal and the oven as a whole relative to the input beam. An additional 3D-stage allows to adjust the crystal position in all three directions of space (x, y, z). The direction of propagation of the fundamental ($\lambda_1 = 1064$nm) and the harmonic ($\lambda_2 = 532$nm) beam is schematically indicated by arrows. (For taking this image the lid of the oven was removed.)

oven is mounted on a mirror mount, which itself is fixed on a 3D movable

stage. Thus the grating of choice can easily be adjusted and you are able to optimize the position of the fundamental beam waist in the crystal.
The oven is connected to a TC200 temperature controller of Thorlabs. It allows to control the temperatures from ambient room temperature up to about 200°C in steps of 0.1°C. The values for the P, I and D parts are programmable and the controller can be operated in two different modes:
In *normal mode* the controller regulates the temperature to the present set value, that can be varied any time.
*Cycle mode* offers the opportunity to program a cycle that consists of up to five steps. During operation you can pause and continue the cycle any time, but it is not possible to change any set value.
As the heating rate should not be faster than 10°C/min to prevent crystal damage cycle mode is chosen to ramp up the crystal from room temperature close to the QPM-temperature, where the cycle is paused. Cycle mode is not useful when you want to fine tune the crystal temperature, so for this purpose it must be changed to normal mode. It is easily possible to change from cycle mode to normal mode.
After the experiment when the crystal should be cooled down, the controller must be changed back to cycle mode again to ramp the crystal down slowly, because otherwise when the controller is just disabled the oven would cool down much faster than the allowed maximum value of 10°C/min (see figure 3.9). Unfortunately it is very unpleasant to change from normal mode to cycle mode because the heater must be disabled, the cycle has to be set and the heater must be enabled quickly again within some seconds.
To provide power at least for the time for ramping down the oven if a power failure happens, an UPS (uninterruptible power supply) is plugged between the mains connection and the TC200. The UPS produces an acoustic signal if a power failure happens and the oven must be ramped down manually.

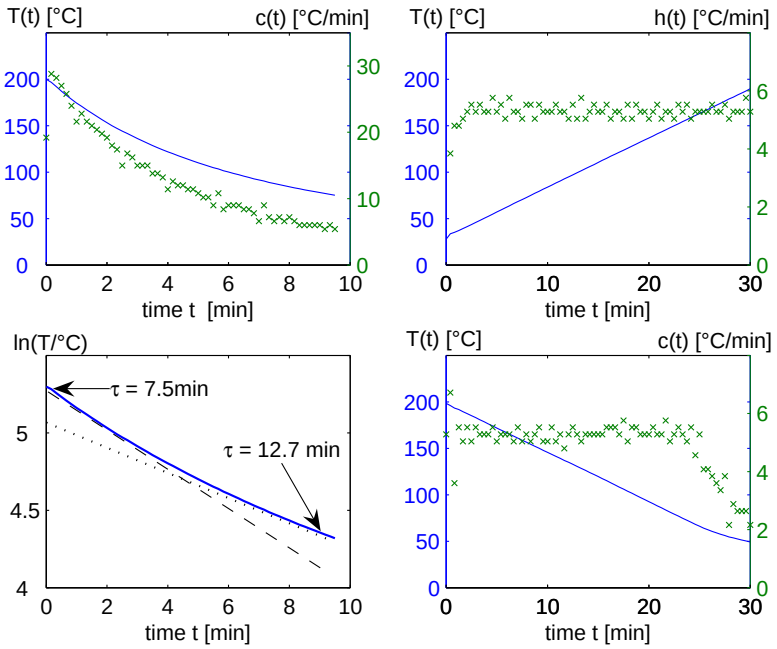


Figure 3.9: *Left top*: The diagram shows the measured thermal relaxation T(t) (solid line, left y-axis) of the oven when the heating element is switched off at a temperature of 200°C. The cooling rate c (crosses, right y-axis) exceeds 10°C/min until the oven temperature is fallen to about 110°C. To prevent damage of the crystal the cooling and heating rate should not be higher than 10°C/min. *Left bottom*: Shown is the thermal relaxation of the oven in a logarithmic plot, from which can be seen that whereas at a oven temperature of about 200°C the oven cools down with a typical cooling time $\tau = 7.5$min (dashed line) at a oven temperature of 80°C it cools down with a typical time $\tau = 12.7$min (dotted line). $\tau$ is determined from exponential fits at the corresponding temperature range. *Right top*: To ramp the crystal temperature T(t) (solid line, left y-axis) up to 200°C in a controlled way a cycle step with starting point at 20°C and an end point of 200°C and a duration of 30min is programmed. The measurement confirms a constant heating rate h (crosses, right y-axis) of about 6°C/min. *Right bottom*: To ramp the oven temperature T(t) (solid line, left y-axis) down to ambient room temperature in a controlled way the reverse cycle (200°C down to 20°C within 30min) is used. The temperature decreases with a rate c(t) (crosses, right y-axis) of about 6°C/min until about 80°C, where no controlled ramping is possible anymore because the oven cannot be cooled actively and the relaxation rate of the oven is smaller than 6°C/min.

## 3.2 Measured dependences of SHG with PPLN

### 3.2.1 Optimized polarization of the fundamental light

The lithium niobate crystal is a dispersive anisotropic nonlinear medium. Its linear optical properties like the refractive index as well as its nonlinear properties like the nonlinear susceptibility $\chi^{(2)}$ depend on the wavelength, the direction of the wave vector and the polarization of a propagating wave in the medium. So describing optics in such a medium in the general case is quite a complex task compared to the case of an isotropic nondispersive medium.
For efficient SHG of a given fundamental wavelength the optimum combination of the wave vector and the polarization of the fundamental light has to be found, so that three important conditions are fulfilled:

- PHASE MATCHING of the fundamental and harmonic wave guarantees that harmonic light generated at different crystal sites interfere positively and a macroscopic harmonic wave can build up.

- Light beams have a limited diameter and it is therefore necessary that fundamental and harmonic beam propagate in the same direction - that is the direction given by the Poynting vector - to allow the macroscopic harmonic wave to be built up over the whole crystal length. Thus WALK OFF between the fundamental and harmonic wave must be prevented.

- Of course the polarization of the fundamental light should be chosen in the direction that offers the highest possible value for the NONLINEAR COEFFICIENT $\chi^{(2)}_{ijk}$ of the medium.

In lithium niobate for example it is possible to prevent walk off and get the highest possible value of the nonlinear susceptibility by choosing the right direction of the wave vector and the right polarization of the fundamental light. Even though due to dispersion in the medium the third necessary condition of phase matching is not fulfilled it is possible to generate harmonic light by Quasi-Phase-Matching (QPM). The crystal is already designed for

this direction of the wave vector but the dependence of the converted power on fundamental light with different linear polarization can be analysed.
In the present setup the fundamental light propagates along a principal axis of the crystal perpendicular to its optical axis and has a polarization parallel to the optical axis of the crystal (see figure 3.2). Thus in the crystal the fundamental light propagates as the extraordinary wave and behaves like it would in an isotropic medium with the wave vector and the Poynting vector aiming in the same direction and its direction of polarization does not change along the crystal.
Because of the chosen polarization of the fundamental light, the only non vanishing part of the nonlinear polarization of the medium $\chi^{(2)}_{333}$ creates harmonic light that propagates along the same direction also with its Poynting vector parallel to its wave vector and constant direction of polarization like the fundamental light. So this direction of the wave vector and this polarization of the fundamental light automatically causes the harmonic and fundamental wave to propagate in the same direction and so walk off is prevented. To check the dependence of the converted power on arbitrary direction of polarization the angle of polarization of the fundamental light is varied by tilting the ($\lambda/2$)-waveplate in front of the crystal and measuring the created green power. Of course for this measurement nether the angle of incidence onto the crystal nor the focusing of the fundamental light was changed and the crystal temperature was held fixed at the optimum temperature.

As can be seen from figure 3.10 the conversion decreases from its best value for fundamental light polarized parallel to the optical axis of the crystal ($\alpha = 0$) down to the lowest value for light polarized perpendicular to the optical axis of the crystal ($\alpha = \pi/2$), where no green light was created at all. For the latter there are two obvious reasons why no harmonic light is converted. Fundamental light with this polarization ($\alpha = \pi/2$) faces smaller nonlinear coefficients $\chi^{(2)}_{311} = 5.95\text{pm/V}$ and $\chi^{(2)}_{211} = 3.07\text{pm/V}$ and its refractive index and thus the dispersion is different, so that the poling length of the grating does not ensure good quasi-phase-matching anymore.
To describe the dependence of the converted power for arbitrary angles of polarization the electric field $E_1$ of the incident fundamental light is split into

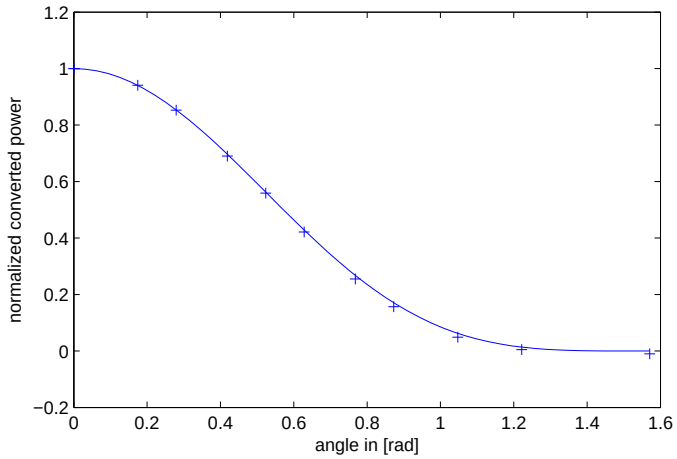


Figure 3.10: Dependence of the converted output power on the polarization of the fundamental light. For fundamental input light of constant power of 1W but different linear polarization the converted output power $P_2(\alpha)$ is measured. The measured values (+) are normalized to the maximum value $P_2(\alpha = 0)$ and plotted against the polarization angle $\alpha$, which is defined as the angle between the direction of the fundamental electric field and the optical axis of the crystal. The straight line shows a calculated $cos^4(\alpha)$-behaviour, which describes the experimental results quite well. From this follows that effectively just the component of the fundamental light that is parallel to the optical axis of the crystal is converted into green light.

the components $E_{1,\parallel}$ and $E_{1,\perp}$ parallel and perpendicular to the optical axis of the crystal respectively. It is assumed that this components can be treated independently from each other, which is not at hoc clear because of the non-linear relation between the harmonic polarization density of the medium and the fundamental electric field (see equation 2.20). Following the assumption above, the generated green power $P_2$ for arbitrary angles of polarization $\alpha$ of the fundamental light can be calculated as:

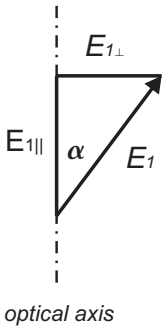


$$P_2 \propto P_{1,\parallel}^2$$

$$P_{1,\parallel} \propto E_{1,\parallel}^2 = (E_1 * \cos\alpha)^2$$

$$\Longrightarrow P_2 \propto \cos^4\alpha$$

This function is plotted together with the normalized measurement results in figure 3.10. The calculated behaviour agrees quite well with the experimental results and thus confirms that the assumption made above is useful to describe the dependence of the converted power on the polarization of the fundamental light.
In conclusion for this PPLN-crystal it is important to polarize the fundamental light parallel to the optical axis of the crystal to achieve the highest possible conversion into green light.
For this polarization the emitted rest of the fundamental light and the generated harmonic light were measured behind the crystal to be polarized parallel to the optical axis of the crystal, as it should be following the explanations

made earlier.

### 3.2.2 Optimum focusing for high conversion

Nonlinear effects like second-harmonic-generation appear when high electric fields $E_1$ of fundamental light are involved. The higher the available intensity of the fundamental light is the more harmonic light is generated. As there is just a limited amount of fundamental power available the electric field is increased by focusing into the crystal.
In this subsection the optimal focusing will be determined and a simple[8] model will be worked out that describes the dependence of conversion on the focusing of the fundamental light. This is done at low power of fundamental light and it is assumed that the results are valid also for high powers.
As the starting point for the development of the model the following situation is considered:
A beam with fundamental frequency $\nu_1$ and a power $P_1$ propagating through the lithium niobate crystal with its wave vector parallel to a principal axis of the crystal. Because the polarization of the fundamental light is choosen parallel to the optical axis of the crystal the wave faces a refractive index $n_1$ and a nonlinear susceptibility $\chi^{(2)}_{333}$. For this case of the wave vector direction and polarization the calculation is equal to the one for an isotropic medium.
The beam diameter of the fundamental beam is supposed to be constant all over the crystal and the intensity is constant anywhere within the fundamental beam, so that there is a flat intensity profile across the beam diameter.
The generated harmonic beam propagates collinearly to the fundamental beam and has the same beam diameter $2\omega$ like the fundamental beam and a flat intensity profile.
The polarization of the harmonic beam is also parallel to the optical axis of the crystal and the refractive index for the harmonic light is $n_2$.
The converted power $P_2$ at the end of the crystal with length $L$ is then given by the generated harmonic intensity $I_2$ from equation 2.13 and the cross

[8] Of course it is possible to calculate the dependence on focusing by brute numerical calculation, but I would like to develop a simple analytic model here and see how far we will get with that.

section area $\pi\omega^2$:

$$P_2 = (2/\pi)^2 I_2 \pi\omega^2 =$$
$$(2/\pi)^2 I_1^2 \frac{2\pi^2\varepsilon_0^2\eta_0^3\nu_1^2 L^2}{n_2 n_1^2} \left(\chi^{(2)}_{333}\right)^2 \pi\omega^2 =$$
$$\frac{P_1^2}{\pi\omega^2} \frac{2\pi^2\varepsilon_0^2\eta_0^3\nu_1^2 L^2}{n_2 n_1^2} \left((2/\pi)\,\chi^{(2)}_{333}\right)^2 \tag{3.2}$$

The factor $2/\pi$ in front of the nonlinear coefficient in the third line accounts for the fact that for QPM the effective nonlinear susceptibility is reduced compared to the case of perfect phase matching (see subsection 2.4.1). As exlained in sections 2.3 and 2.5 $\chi^{(2)}_{333}$ was used as the relevant nonlinear susceptibility. In the last line the relation for the fundamental intensity $I_1 = P_1/(\pi\omega^2)$ was used.

Of course the fundamental power decreases along the crystal when harmonic light is created but as long as the converted power can be neglected compared to the fundamental power the assumption of a fundamental beam with constant power all along the crystal will be valid. So concerning this the above calculation should give a good approximation because we want to optimize the focusing at low fundamental power anyway.

The model so far predicts that the converted power $P_2$ increases if the diameter of the beam decreases. (Note that in the last line $\pi\omega^2$ is in the nominator.) The explanation for this is that the smaller the beam diameter is prepared the higher gets the intensity and thus the nonlinear polarization of the medium as the source for the harmonic light increases and more harmonic light is generated.

This is valid as long as the diameter of the beam is constant all over the crystal, which is the case when the fundamental beam is loosely focused into the crystal. But when the focusing is tight we must take Gaussian optics into account. As waist $\omega_0$ and divergence $\omega_0/z_0$ of a beam are interrelated by $\omega_0 \frac{\omega_0}{z_0} = \lambda/\pi$ it follows that the smaller the waist of a beam the higher its divergence will be. So for tight focusing the intensity in vicinity of the waist is high but outside the waist the intensity drops down quickly. Consequently

the local conversion in vicinity of the waist increases but summed over the whole crystal conversion would decrease when the focusing is too tight.

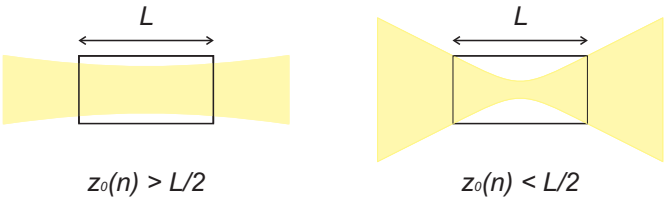


Figure 3.11: When Gaussian optics is taken into account the focusing of the fundamental beam can be optimized. *Left*: When the fundamental beam is loosely focused into the crystal its divergence is low and it propagates through the medium like a beam with constant beam diameter. As the beam diameter is big the intensity of the fundamental light inside the crystal is low and thus conversion is small. *Right*: When the focusing of the fundamental beam is too tight, the intensity at the waist is high but due to the high divergence the intensity drops down outside the Rayleigh range. Effectively not the whole crystal length is used for conversion.

Thus there should be an optimum focusing somewhere between loose and too tight focusing that offers a compromise between a small waist and a small divergence.
In a first approximation the Rayleigh range of a beam is seen as the region that due to its high intensity generates all of the harmonic power. Then for a rough estimation of the optimum focusing it is assumed, that the fundamental beam should be prepared in the way, that its Rayleigh length $z_0(n)$ equals half the crystal length. When the refractive index $n$ of the medium is taken into account the corresponding waist can be calculated as:

$$z_0(n) = n\frac{\omega_0^2\pi}{\lambda} \tag{3.3}$$

Where $n$ denotes the refractive index in the medium for the corresponding wave with the wavelength $\lambda$.

$$\longrightarrow \omega_0^2 = \frac{z_0(n)\lambda}{n\pi} = \frac{(L/2)\lambda_1}{n_1\pi} = \approx (40\mu m)^2$$

Where $L = 2\text{cm}$, $\lambda_1 = 1064\text{nm}$ and $n_1 = 2.17$. This estimated value of $\omega_0 = 40\mu\text{m}$ for the optimum waist differs from the experimentally obtained value of about $\omega_{0,opt} = 30\mu\text{m}$, which shows that the optimum waist is smaller than the one estimated by the model above. The experimental results are plotted in figure 3.12.

It would be fine if the optimum waist could be estimated more accurately and if the dependence of the converted power on the focusing could be described for loose and for tight focusing at once. For that purposes the model above will be improved in the following.

On the one hand it is clear that a beam with a big beam diameter lacks in intensity and thus conversion is low. On the other hand too tight focusing causes - due to the involved large divergence of the beam - an increasing beam diameter outside the Rayleigh range, so that the intensity outside the focus is too low to contribute considerably to the generated harmonic power. That is why I try to take both facts into account by substituting in the model above (equation 3.2) the averaged intensity $\langle I_1 \rangle$ of a Gaussian beam with given waist $\omega_0$ for the constant beam intensity $I_1$, and the averaged cross-section area $\pi \langle \omega^2 \rangle$ of the Gaussian beam for the constant cross-section area $\pi\omega^2$.[9] The improved model then becomes:

$$P_2 = \langle I_1 \rangle^2 \frac{2\pi^2 \varepsilon_0^2 \eta_0^3 \nu_1^2 L^2}{n_2 n_1^2} \left( (2/\pi)\, \chi^{(2)}_{333} \right)^2 \pi \langle \omega^2 \rangle = \frac{P_1^2}{\pi \langle \omega^2 \rangle} \frac{2\pi^2 \varepsilon_0^2 \eta_0^3 \nu_1^2 L^2}{n_2 n_1^2} \left( (2/\pi)\, \chi^{(2)}_{333} \right)^2 \tag{3.4}$$

In the last line the relation for the fundamental intensity $\langle I_1 \rangle = P_1/(\pi \langle \omega^2 \rangle)$ was used, which brings $\pi \langle \omega^2 \rangle$ into the nominator. The average square $\langle \omega^2 \rangle$ of the beam radius over the whole crystal length $L$ is calculated with the assumption for the beam radius $\omega(z) = \omega_0 \sqrt{1 + (z/z_0)^2}$ by:

[9] At this time doing so is just a guess. The comparison with the experimental results later on will show if this was a good guess.

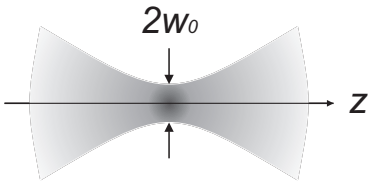


$$\left\langle \omega^2 \right\rangle := \left\langle \omega^2(\omega_0) \right\rangle = \frac{2}{L} \int_0^{L/2} (\omega(z))^2 dz = \omega_0^2 \left( 1 + \frac{1}{12} \left( \frac{L}{z_0(n)} \right)^2 \right) = \omega_0^2 + \frac{1}{12} \left( \frac{L\lambda_1}{n_1 \omega_0 \pi} \right)^2 \tag{3.5}$$

To yield the result in the last line the relation 3.3 between waist $\omega_0$ and the Rayleigh length $z_0(n)$ for a beam with wavelength $\lambda$ in a medium with refractive index $n$ was used, where $\lambda = \lambda_1 = 1064\text{nm}$ and $n = n_1 = 2.17$. The calculated behaviour (equation 3.4) is plotted with the experimental results in figure 3.12, thereby $\chi^{(2)}_{333}$ was used as a fit parameter. A least-square fit was implemented to determine the best value for this single fit parameter. From this fit the value for the nonlinear coefficient $\chi^{(2)}_{333} = 33\text{pm/V}$ was obtained, which agrees within the error bars quite well with the corresponding value of $\chi^{(2)}_{333} = 34\text{pm/V}$ for lithium niobate given in [33].

In the vicinity of the optimum waist the new model predicts the measurement results quite well. The experimentally found optimum waist $\omega_{opt} = 30\mu m$ can also be calculated by the new model. Due to the dependence of the generated harmonic power $P_2$ (equation 3.4) on $\langle \omega^2 \rangle$, which depends on the waist $\omega_0$ of the focused fundamental beam, the optimum waist must fulfill the condition[10]:

$$\frac{d}{d\omega_0} \left\langle \omega^2(\omega_0) \right\rangle = \frac{d}{d\omega_0} \left( \omega_0^2 + \frac{1}{12} \left( \frac{L\lambda_1}{n_1 \omega_0 \pi} \right)^2 \right) := 0$$

From this necessary condition the optimum waist can further be calculated

[10]This condition is simply obtained by determining the extremum of $P_2(\omega_0)$ from equation 3.4.

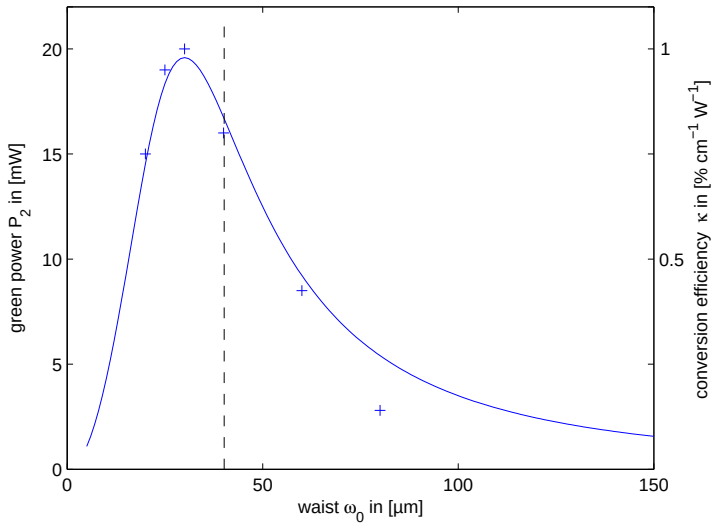


Figure 3.12: The dependence of the converted power $P_2$ on the focusing of the fundamental input beam shows an optimum at a waist $\omega_{0,opt} = 30\mu m$. For the measurement a constant fundamental input power $P_1 = 1W$ is used. The solid line shows the calculated results obtained with the model described in the text with the value for the nonlinear coefficient $\chi^{(2)}_{333} = 33pm/V$. The model takes Gaussian optics into account. Choosing the focusing in the way that the Rayleigh length of the fundamental beam in the crystal is half the crystal length is a good rule of thumb to get a rough estimation for the optimum waist (this estimated value of $\omega_0 = 40\mu m$ is marked by the dotted vertical line in the diagram). The right y-axis gives the corresponding values for the conversion efficiency $\kappa := P_2/(P_1^2 L)$, with the crystal length $L = 2$cm.

to:

$$\longrightarrow 2\omega_0 - \frac{2}{12}\frac{1}{\omega_0^3}\left(\frac{L\lambda_1}{n_1\pi}\right)^2 = 0$$

$$\longrightarrow \omega_{0,opt} = \sqrt[4]{\frac{1}{12}\left(\frac{L\lambda_1}{n_1\pi}\right)^2} =$$

$$\sqrt[4]{\frac{1}{12}\left(\frac{2*10^4*1.064}{2.17*\pi}\right)^2}\,\mu m \approx 30\mu m$$

When using the optimum focusing for powers of the fundamental light up to 10W, the damage threshold of the crystal given by 0.5MW/cm$^2$ should not be exceeded. For a fundamental power of 10W and a beam waist of $\omega_{0,opt} = 30\mu$m an averaged intensity of $P_1/(\pi\,\langle\omega^2(\omega_{0,opt})\rangle) \approx 0.2$MW/cm$^2$and a peak intensity directly at the waist of $2P_1/(\pi\omega_{0,opt}^2) \approx 0.7$MW/cm$^2$ are calculated. In the latter a Gaussian beam profile was assumed.
Unfortunately these values are quite close to and above the lower limit of the damage threshold and thus the crystal must be handled carefully when high powers of fundamental light are involved (see section 3.2.4).
The achieved conversion efficiency near optimum focusing is calculated from the measurement results to about $\kappa := P_2/(P_1^2 L) = 0.01\text{W}^{-1}\text{cm}^{-1}$, where the used values are $P_2 = 0.02$W, $P_1 = 1$W and $L = 2$cm. This agrees with the value of $\kappa = 0.01\text{W}^{-1}\text{cm}^{-1}$ given by the manufacturer. As will be shown in section 3.2.4 this conversion efficiency determined at a fundamental power of 1W decreases when higher powers of fundamental light are used.
For experimental reasons it is also interesting to know how good the optimum waist must be prepared to ensure conversion close to the optimum value. To formulate a general statement on this issue the new model is used again to get a relation between deviation from the optimum waist and the resulting deviation from the optimum conversion efficiency[11]: From figure 3.12 is seen, that the harmonic power $P_2$ and thus the conversion efficiency $\kappa$ depends on the focusing. A Taylor's series expansion around the optimum waist $\omega_{0,opt}$ leads to:

[11]Even though the following calculation looks daunting at the first sight, the calculus follows simple principles, so hang on.

$$\Delta\kappa = \underbrace{\left[\frac{\partial\kappa}{\partial\omega_0}\right]_{\omega_0=\omega_{0,opt}}}_{0}\Delta\omega_0 + \left[\frac{\partial^2\kappa}{\partial\omega_0^2}\right]_{\omega_0=\omega_{0,opt}}(\Delta\omega_0)^2$$

The first partial derivative of $\kappa$ vanishes, which is a necessary condition for an extremum. The second partial derivative of $\kappa$ can be calculated by use of equation 3.4, so

$$\kappa \propto \frac{1}{\langle\omega^2\rangle} \Longrightarrow \left[\frac{\partial^2\kappa}{\partial\omega_0^2}\right]_{\omega_0=\omega_{0,opt}} \propto -\frac{1}{\langle\omega^2(\omega_{0,opt})\rangle^2}\underbrace{\left(\frac{\partial^2}{\partial\omega_0^2}\langle\omega^2(\omega_0)\rangle\right)_{\omega_0=\omega_{0,opt}}}_{\approx 8}$$

Now having $\Delta\kappa$ the relative deviation of the conversion efficiency is calculated to

$$\Longrightarrow |\Delta\kappa/\kappa(\omega_{0,opt})| = \frac{8\,(\Delta\omega_0)^2}{\langle\omega^2(\omega_{0,opt})\rangle^2}\Big/\frac{1}{\langle\omega^2(\omega_{0,opt})\rangle} = 4\left(\frac{\Delta\omega_0}{\omega_{0,opt}}\right)^2$$

Inserting some numbers into this relation it follows that for a conversion efficiency, which should not deviate by more than 5% from the optimum value, the waist of the fundamental beam must be in the range of $\pm 10\%$ of the optimum waist. From this the necessary requirements on the optic elements and the stability of the setup can be deduced.

For the measurement in figure 3.12 first the relevant parameters of the fundamental beam delivered by the fiber-amplifier were determined. The beam is slightly divergent with a full divergence angle of about 2mrad and has a beam diameter at the position of the focusing lens of $D = (1800 \pm 200)\mu$m. A fundamental input power of 1W was chosen, that was tested to be low enough not to damage the crystal but that was high enough to get a good signal even for not optimized focusing.

For the measurements in figure 3.12 lenses of different focal lengths were used to prepare different waists and the fundamental power, the crystal temperature and the direction of polarization parallel to the optical axis of the crystal were held constant. The respective values of the waists were calculated by the formula for diffraction limited focusing and the position of each waist was determined with the waist meter. The calculated waists are listed in the

| $f$ *in mm* | $\omega_0$ *in* $\mu m$ * |
|---|---|
| 50 | 20 |
| 75 | 30 |
| 100 | 40 |
| 150 | 60 |
| 200 | 80 |

Table 3.1: For the different focusing lenses with focal length $f$ the calculated waists $\omega_0$ are listed.(∗...calculated for diffraction limited focusing $\omega_0 \geq \frac{2\lambda}{\pi D} f$, $\lambda = 1064$nm ...fundamental wavelength, $D = 1800\mu$m ...beam diameter at lens position)

table 3.1.

Crystal and oven as a whole were first placed at this position and fixed on the optical table, the degrees of freedom of the oven mount then were used to adjust the fundamental beam through the grating and to fine tune the crystal orientation and position for maximizing the converted power. The accuracy with which the position of the waist inside the crystal has to be adjusted in the direction of beam propagation depends on the focusing. For loose focusing this adjustment is not as critical as for tight focusing as can be seen in figure 3.13. This dependence is also predicted by the model above (compare equation 3.4). The solid lines in figure 3.13 correspond to the values calculated by the same model, but now the term $\langle \omega^2(\omega_0) \rangle$ is substituted by the more general term $\langle \omega^2(\omega_0, \Delta z) \rangle$ - the averaged value of the squared beam radius over the whole crystal length $L$ for a Gaussian beam of waist $\omega_0$ that is displaced from the middle of the crystal by the distance $\Delta z$:

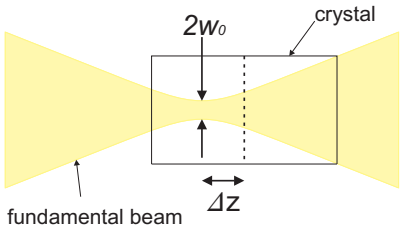


The average square of the beam radius along the whole crystal with

$w(z) = w_0\sqrt{1+(z/z_0)^2}$ is then

$$\left\langle \omega^2(\omega_0, \Delta z) \right\rangle := \frac{1}{L}\int_{-L/2-\Delta z}^{+L/2+\Delta z} (\omega(z))^2 dz =$$

$$\frac{1}{L}\left(\int_0^{+L/2+\Delta z} \omega^2(z)dz + \int_0^{+L/2-\Delta z} \omega^2(z)dz\right) = ...$$

$$\omega_0^2\left(1+\frac{1}{12}\left(\frac{L}{z_0(n)}\right)^2\right) + \omega_0^2\left(\frac{\Delta z}{z_0(n)}\right)^2$$

In comparison to $\langle\omega^2\rangle$ from equation 3.5 the second term in the last line displays the effect of the deadjustment $\Delta z$. So a deviation from the optimum adjustment (when the focus is in the middle of the crystal) results in a larger average cross section area of the fundamental beam and thus a lower conversion.

In this subsection a model was worked out that allows to describe the dependence of the generated harmonic power on the focusing of the fundamental beam. For the 20mm long PPLN-crystal the optimum waist $\omega_{0,opt} = 30\mu$m was found for a fundamental power of 1W at the wavelength of 1064nm. For this focusing and this fundamental power a conversion efficiency of $\kappa = 0.01\text{W}^{-1}\text{cm}^{-1}$ was achieved. This waist will also be used for fundamental light power of up to 10W. It was not tested if the optimum focusing depends on the fundamental input power level. Such a dependence could perhaps arise from effects that were not considered here like pump depletion or temperature gradients due to local heating of the crystal by absorption.

### 3.2.3 Dependence of QPM on the crystal temperature for different powers of fundamental light. An evidence of GRIIRA.

To achieve Quasi-Phase-Matching in lithium niobate of the fundamental and harmonic wave the nonlinear susceptibility is periodically modulated by periodically poling of the ferro-electric medium. This inverts the crystal structure

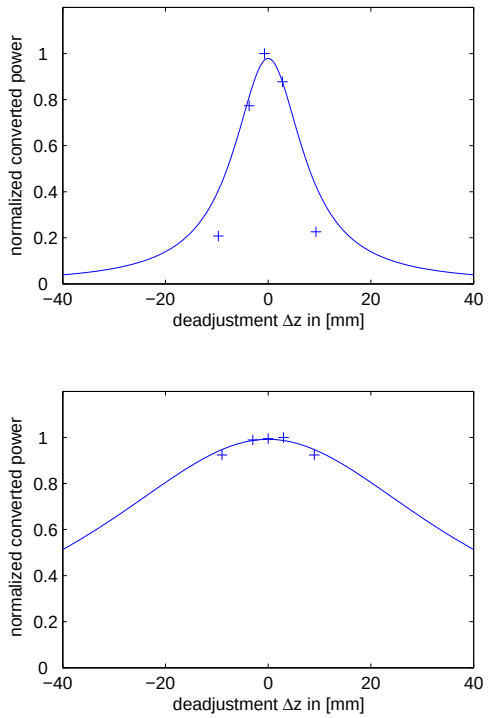


Figure 3.13: The accuracy with which the waist must be adjusted inside the crystal along the beam propagation axis depends on the focusing of the fundamental beam. The diagrams show the dependence of the converted power on the detuning from the optimum waist-position (waist in the middle of the crystal). The plotted values are normalized to the corresponding peak value. (+) denotes measurement results whereas the solid line are calculations obtained with the model explained in the text. *Top*: For optimal focusing $\omega_{0,opt} = 30\mu$m the full half width of the conversion peak is about 16mm and to ensure a conversion that is within 5% of the optimum value the waist must be adjusted with an accuracy of about $\pm$2mm relative to the optimum position. *Bottom*: For loose focusing $\omega_0 = 80\mu$m the full half width of the conversion peak is about 80mm and to ensure a conversion that is within 5% of the optimum value the waist must be adjusted with an accuracy of about $\pm$1cm relative to the optimum position. Thus for tighter focusing the adjustment of the waist is more critical than for loose focusing.

of neighbouring damains and so causes the nonlinar coefficient to change sign periodically (see section 2.5).
It is important that the condition (equation 2.12) between the coherence length $l_c$, the fundamental wavelength $\lambda_1$ and the refractive indices $n_1$ of the fundamental light and $n_2$ of the harmonic light is fulfilled (see sections 2.2.1 and 2.4.1):

$$l_c = \frac{2\pi}{|\Delta k|} = \frac{2\pi}{|k_2 - 2k_1|} = \frac{\lambda_1}{2\,|n_2 - n_1|} = \frac{\lambda_1}{2\Delta n}$$

This guarantees even in a dispersive medium that the created harmonic fields from neighbouring domains interfere constructively and a macroscopic wave of green light can build up.
The gratings on the PPLN-crystal in this setup have period lengths that allow frequency doubling of fundamental light with a wavelength between 1059.8nm and 1067.6nm. To fulfill the QPM-condition (equation 2.12) for a given fundamental wavelength within this range the only parameter that must be adjusted is $\Delta n$ - the difference between the refractive indices of fundamental and harmonic light.
As the refractive index changes differently with temperature for different wavelengths, $\Delta n$ is temperature dependent and the necessary value for $\Delta n(T)$ can be adjusted by varying the crystal temperature. Thermal expansion of the crystal with a relative thermal expansion coefficient in the order of $10^{-6}/°\mathrm{C}$ [12] can be neglected in comparison to the relative change of $\Delta n$ with temperature. The latter can be estimated from figure 3.14 as $(\partial(\Delta n)/\partial T)(1/\Delta n) \approx= 3 * 10^{-4}/°\mathrm{C}$. In figure 3.14 the temperature dependence of $\Delta n = n_2 - n_1$ for the wavelengths of 532nm and 1064nm is shown. The corresponding values for the extraordinary refractive indices $n_1$ and $n_2$ were calculated by the temperature dependent Sellmeier-equation given in section 2.5.
For the three gratings on the crystal and the fundamental wavelength of $\lambda_1 = 1064\mathrm{nm}$ the necessary values of $\Delta n$ calculated with formula 2.12 and the expected QPM temperatures taken from figure 3.14 are listed in table

[12] This value is given by [33] at a temperature of 25°C. Here it is assumed that the value of the thermal expansion coefficient does not change much for a temperature of 200°C.

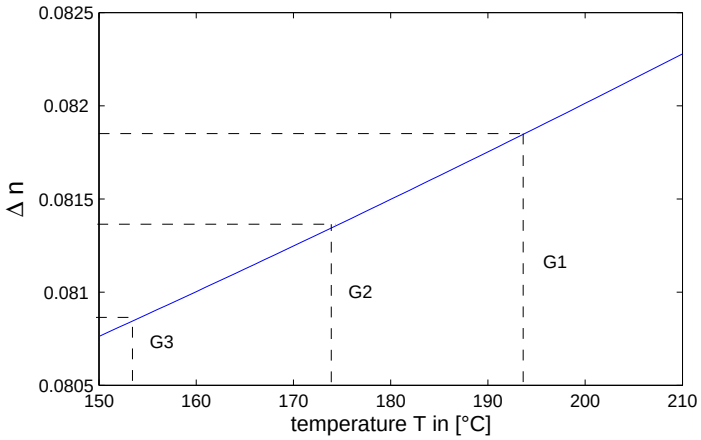


Figure 3.14: The difference of the refractive indices between fundamental and harmonic wave $\Delta n = n_2 - n_1$ increases with temperature nearly linearly in the plotted range with a slope $\partial(\Delta n)/\partial T \approx 0.0012/(48°C) = 0.25 * 10^{-4}/°\mathrm{C}$. The temperature dependent extraordinary refractive indices $n_1$ and $n_2$ are calculated by the Sellmeier-equation in section 2.5. The relative change of $\Delta n$ with temperature is estimated as $(\partial(\Delta n)/\partial T)(1/\Delta n) \approx 3 * 10^{-4}/°\mathrm{C}$, where $\partial(\Delta n)/\partial T = 0.25 * 10^{-4}$ °C and $\Delta n \approx 0.081$ was used. This estimation for the relative change of $\Delta n$ is larger than the thermal expansion coefficient of $2 * 10^{-6}/°\mathrm{C}$. Thus fulfilling relation 2.12 for QPM is mainly accomplished by the temperature dependence of the refractive index difference $\Delta n$ and not due to thermal expansion of the crystal. For each af the three gratings (G1, G2, G3) on the crystal the necessary refractive index difference $\Delta n$ - calculated by formula 2.12- and the corresponding QPM-temperature are marked in the diagram.

| $\boldsymbol{G\sharp}$ | $l_c$ ***in*** $\mu m$ | $\Delta n$ * | $T_{QPM}$ ***in*** $°C$ ** |
|---|---|---|---|
| G3 | 6.58 | 0.08085 | 154 |
| G2 | 6.54 | 0.08135 | 174 |
| G1 | 6.50 | 0.08185 | 194 |

Table 3.2: For the different gratings the necessary difference of the refractive indices $\Delta n$ and the resulting QPM-temperature $T_{QPM}$ are listed.(G♯...grating number, $l_c$...poling length, $*$...calculated value with formula 2.12, $**$...measured from figure 3.14)

3.2.

The period lengths of the gratings are designed to allow quasi-phase-matching at elevated crystal temperatures between 160°C and 200°C. At such high temperatures the crystal is prevented of photo-refractive damage (see section 2.5), because at high temperature charge carriers, which are generated by the incident light, have a higher mobility and recombine faster so that no internal field, that otherwise could affect the refractive index via the electro-optic effect, can build up.
There are also different methods how the photo-refractive effect can be prevented. For example doping lithium niobate with Mg allows second-harmonic generation at about room temperature ([35]).

Experimentally the temperature dependence of the converted power for the corresponding grating was measured by scanning the crystal temperature and measuring the harmonic green power. All other relevant parameters like the focusing, the fundamental power and the polarization angle were held constant. The temperature was ramped with a rate of about 0.4°C/min - slow enough to allow the crystal to thermalize. The results of this measurement are displayed in figure 3.15.
The measured QPM-temperatures for the individual gratings of about 163.5°C, 182.5°C and 202°C differ by about 10°C from the theoretical predicted values of 154°C, 174°C and 194°C. A possible reason for this quite big difference is explained in the following: As the predictions from theory should be precise enough and as the temperature measurement was proved to be reliable this means that the measured temperature does not correspond to the ac-

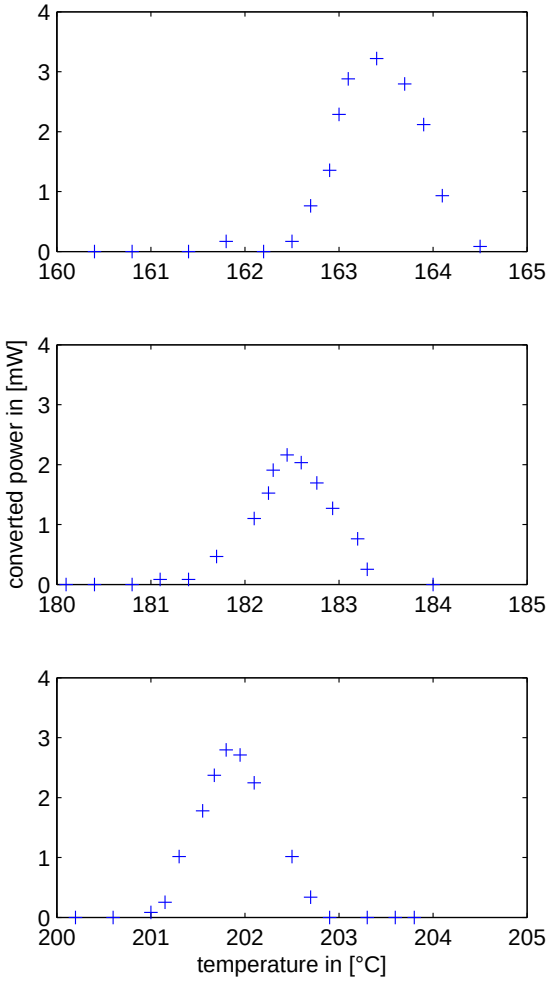


Figure 3.15: On the crystal there are three gratings (G1, G2, G3) with different poling periods $l_c$ (6.50$\mu$m, 6.54$\mu$m, 6.58$\mu$m respectively) resulting in three different QPM-temperatures, which are measured as 202°C, 182.5°C and 163.5°C respectively. For a constant fundamental input power $P_1 = 1$W and loose focusing of $\omega_0 = 80\mu$m the converted output power $P_2$ in the vicinity of the individual QPM-temperature is shown.

tual crystal temperature that is measured. The temperature difference could arise from the fact that the temperature resistor is placed at the socket of the crystal's heating plate and is thus not close to the crystal. So strictly speaking it is the socket temperature that is measured and regulated by the PID.
As the heating plate of the oven and the alignment body of the clip are made of gold coated copper with a high thermal conductivity this temperature gradient must arise because of a bad thermal contact between heating plate and alignment body, which are just pressed onto each other by retaining bolts on the top of the oven. There cannot be used thermal compound to increase the thermal conductivity because evaporated material could saddle down at the crystal facets and could lead to crystal damage when high powers of fundamental light are used.
The temperature range in which the conversion does not vanish can be measured from figure 3.15 to be approximately 2°C for any grating. This value agrees with the following theoretical calculation: From figure 2.2 in section 2.2.1 the full width for efficient conversion is obtained:

$$\delta(\Delta k) = \frac{4\pi}{L}$$

From equation 2.12 can be seen, that $\Delta k$ is connected to $\Delta n$ by:

$$\Delta k = \frac{4\pi}{\lambda_1}\Delta n$$

And thus the differential is given by:

$$\delta(\Delta n) = \frac{\lambda_1}{4\pi}\delta(\Delta k)$$

The change of $\Delta n$ is caused by a change of the crystal temperature T, so that for small changes it is legal to use:

$$\delta(\Delta n) = \frac{\partial(\Delta n)}{\partial T}\Delta T$$

where $\partial(\Delta n)/\partial T = 0.25 * 10^{-4}/°\mathrm{C}$ is obtained from figure 3.14. Putting all together results in a relation between $\delta(\Delta k)$ and $\Delta T$:

$$\delta(\Delta n) = \frac{\lambda_1}{4\pi}\delta(\Delta k) = \frac{\partial(\Delta n)}{\partial T}\Delta T$$

With $\delta(\Delta k) = 4\pi/L$ and $\partial(\Delta n)/\Delta T = 0.25 * 10^{-4}/°\mathrm{C}$ the corresponding temperature range $\Delta T \approx 2°\mathrm{C}$ for efficient conversion is determined.
In principle the QPM-temperature for any of the gratings on the crystal should be independent of the fundamental pump power. To prove this the dependence of conversion on temperature was determined for grating G1 with a period length of 6.50$\mu$m for fundamental pump powers of 1W and 10W respectively.
The conversion efficiencys $\kappa$ for each of the two fundamental powers are plotted against the measured temperature in figure 3.16, where the conversion efficiency is defined through:

$$P_2 = \kappa P_1^2 L \tag{3.6}$$

The optimum conversion efficiencys are about $1\%\mathrm{W}^{-1}\mathrm{cm}^{-1}$ and $0.7\%\mathrm{W}^{-1}\mathrm{cm}^{-1}$ (see section 3.2.4) for pump power of 1W and 10W respectively. The decrease of the conversion efficiency for high pump powers can be explained by pump depletion. Each photon of harmonic light that is generated costs two photons of fundamental light. So an increase of harmonic light along the crystal goes along with a decrease of fundamental light toward the crystal end. Of course a reduced fundamental power causes less harmonic power to be generated and the green output power will not increase with the square of the fundamental input power anymore. This is considered in the above definition of $\kappa$ by allowing the conversion efficiency to be a decreasing function of the fundamental input power (see section 3.2.4).
Both curves in figure 3.16 show nearly the same full width of 2°C. So the relevant temperature range for conversion seems to be independent of the fundamental input power.

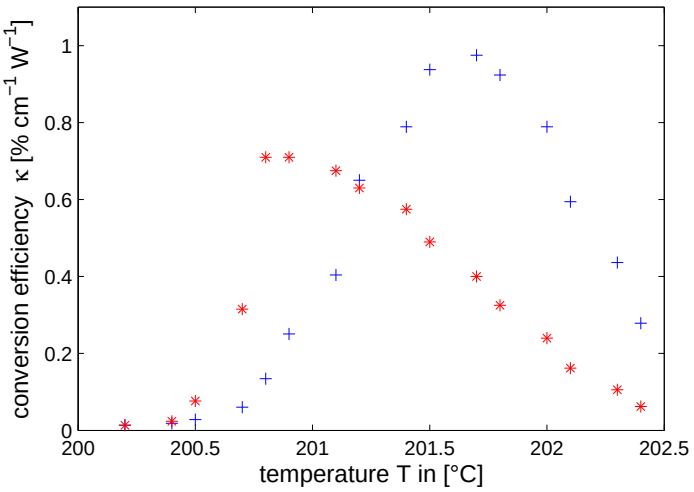


Figure 3.16: For two different powers of the fundamental input light ($P_1 =$ 1W(+), $P_1 = 10$W($*$)) and for grating G1 the temperature is scanned in the vicinity of the optimum temperature and the effective conversion efficiency $\kappa$ is determined ($P_2 = \kappa P_1^2 L$). Here the fundamental beam is focused to a waist $\omega_0 = 30\mu$m (optimal focusing). The optimum temperature for a fundamental input power $P_1 = 10$W is about 1°C lower than the one for $P_1 = 1$W (details are explained in the text).

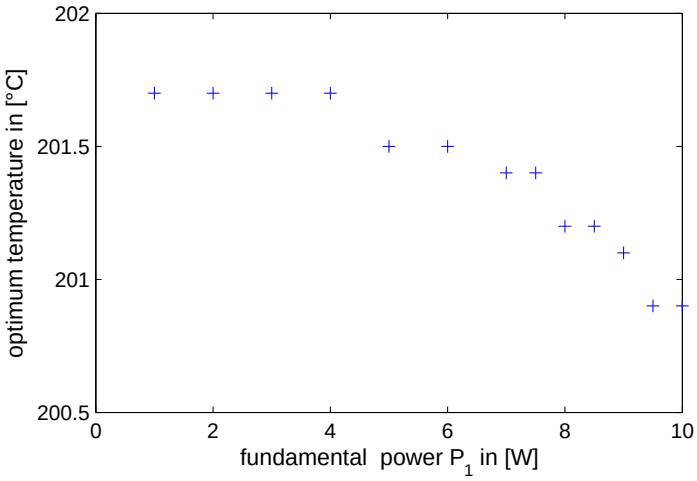


Figure 3.17: The graph displays the measured optimum temperatures for different fundamental input powers $P_1$. The optimum temperature decreases as the fundamental input power increases.

In contradiction to expectations made above the optimum temperature [13] for a fundamental input power of 10W is found to be about 1°C lower than the one for a fundamental input power of 1W.
This can be attributed again to the bad thermal contact between the alignment body and the heating plate explained above. On the one hand this bad control of the temperature is not pleasant but on the other hand it provides an evidence for the appearance of heating effects inside the crystal at high fundamental powers.
The decreasing behaviour of the measured optimum temperature with increasing fundamental input power is illustrated in figure 3.17:
Responsible for the heating of the crystal is simple absorption of the fundamental and harmonic light - which should be small because the two wavelengths are within the transparency range of lithium niobate given by (420-5200)nm - and also responsible is the effect of Green-Induced-InfraRed-Absorption (GRIIRA): In the ground state, IR-absorption is low, but when green light, which has a higher coefficient of absorption than the IR-light, is

[13]The temperature that is measured by the PT100 at the heating plate.

present the atoms are excited into a state in which they can then absorb the IR light (see also section 2.5).
The appearance of GRIIRA can thus be proved by detecting an increased loss of fundamental power at the output when green light is present inside the crystal. As the absorbed power cannot be measured directly it is in the following calculated from quantities that can be measured directly:
Because energy is conserved at any time it is possible to deduce that the incident fundamental power $P_1$ must be shared out completely between the output channels of the system. These output channels are:

- the power of harmonic light $P_2$ that is generated,
- the rest of the fundamental light $P_{1,rest}$ in the end of the crystal
- and the power $P_{missing}$ that is necessary to fulfill energy conservation and that will be identified later on as the power of IR-light that is absorbed by GRIIRA.

So at the crystal end but still inside the crystal the following equation should hold:

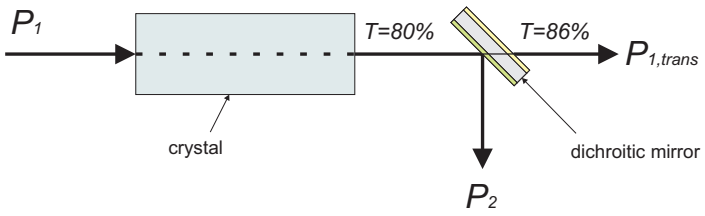


$$P_1 = P_2 + P_{1,rest} + P_{missing}$$

$$\text{where } P_{1,rest} = \frac{P_{1,trans}}{0.86*0.8}$$

$$\longrightarrow P_{missing} = P_{1,input} - P_2 - \frac{P_{1,trans}}{0.86 * 0.8}$$

Where $P_{1,rest}$ is determined by the fundamental power $P_{1,trans}$ that is measured behind the dichroitic mirror, which has a measured transmission of

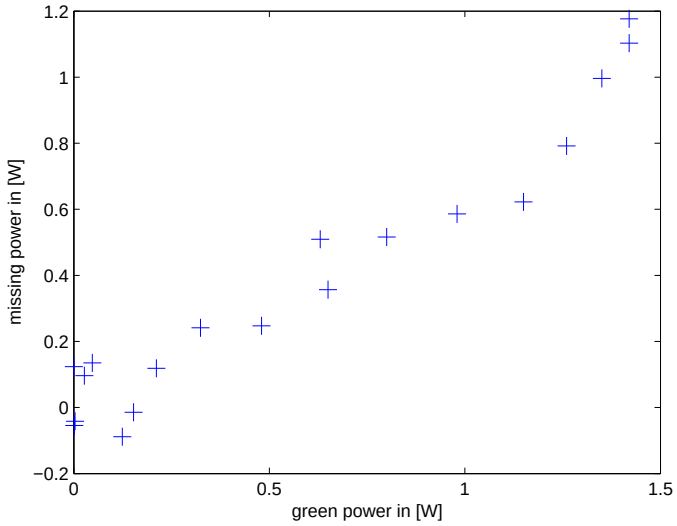


Figure 3.18: The measurement shows the dependence of the missing fundamental power on the converted power of green light $P_2$ present. A fundamental input power $P_1 = 10$W is used and the green power $P_2$ is varied by detuning the crystal temperature. Due to GRIIRA the missing IR power increases with increasing green power.

$T = 86\%$ at the fundamental wavelength of 1064nm, and by the measured transmission of the crystal's output facet. The latter was measured to $T = 80\%$ at the fundamental wavelength.
The input facet is AR-coated for the fundamental wavelength and thus losses because of rest-reflectivity are neglected here.
In a measurement series the fundamental input power of 10W was held constant and the corresponding values of the created green power $P_2$ and the fundamental power $P_{1,trans}$ were measured. $P_2$ was varied between no green light and up to about 1.4W of green light by adjusting the crystal temperature from far off up to the QPM-temperature.
The values for the power $P_{missing}$, calculated by these measurement results are plotted in figure 3.18 against the corresponding power of green light $P_2$.
The diagram illustrates that $P_{missing}$ increases from about zero up to about 1W for increasing power of green light. When there is no green light present

$P_{missing}$ is expected to have a value of about $P_{missing}(T_{faroff}) = \alpha L P_1 = 0.001 * 2 * 10 = 0.02$W due to *simple* absorption of fundamental light, where the absorption coefficient in lithium niobate is given by $\alpha = 0.1\%/\text{cm}$ [33] at 1064nm. This value agrees with the corresponding measurement result in figure 3.18 within the error bars.
The increased loss of power when green light is present cannot be explained by *simple* absorption because the necessary absorption coefficient would be too high.
*Simple* absorption of green light can also be excluded, because if 1W of green light would be absorbed an averaged absorption coefficient of
$\alpha$ =1W/((1+1.4)W*2cm)=21%/cm for green light follows. In consideration of the fact that the harmonic wavelength lies within the transparency range of lithium niobate, that is given by (420-5200)nm, this value is much to high. Beside this the whole generated green power $P_{2,ges} = P_2 + P_{missing}$ ≈1.4W + 1W = 2.4W would clearly exceed the theoretically predicted value of 1.7W (see section 3.2.4).
Therefore the increased absorption of the fundamental light when green light is present can be ascribed to the GRIIRA-effect in lithium niobate.
GRIIRA could disturb second-harmonic-generation in many ways:
Green light that has already been created is absorbed and due to the increased absorption of IR-light the intensity of the fundamental light is reduced and thus causes that less harmonic light is generated.
As the absorption of IR-light increases with increasing green power and as the green power grows along the crystal (see subsections 2.2.1 and 2.2.2) the heating rate along the crystal is not the same and a temperature gradient along the crystal can build up. At certain places the crystal temperature thus may differ from the QPM-temperature leading to a lower conversion.

### 3.2.4 Harmonic power as function of fundamental power

As already mentioned earlier, conversion gets better the higher the available intensity of the fundamental light is. The optimum waist thus has already been determined to $\omega_0 = 30\mu m$ at a low fundamental power of 1W and this

focusing will now also be used for high fundamental input power because it is not expected that effects like GRIIRA or thermal lensing that appear at high powers will significantly affect the optimum focusing.
For this focusing the intensity can be increased further by simply raising up the fundamental power.
As long as the created harmonic power can be neglected compared to the fundamental pump power the converted power will follow the model (equation 3.4) developed in subsection 3.2.2 and grows with the square of the fundamental pump power:

$$P_2 = \frac{2\pi^2 \varepsilon_0^2 \eta_0^3 \nu_1^2}{n_2 n_1^2} \left( (2/\pi)\, \chi_{333}^{(2)} \right)^2 \frac{L^2 P_1^2}{\pi \left\langle \omega^2 \right\rangle} = \kappa L P_1^2$$

$$\kappa = \frac{2\pi^2 \varepsilon_0^2 \eta_0^3 \nu_1^2}{n_2 n_1^2} \left( (2/\pi)\, \chi_{333}^{(2)} \right)^2 \frac{L}{\pi \left\langle \omega^2 \right\rangle}$$

Although for QPM in a microscopic view fundamental and harmonic wave are not phase matched, it can in the macroscopic view be treated formally as the case for a crystal providing perfect phase matching but with a reduced nonlinear susceptibility coefficient $\chi_{eff}^{(2)} = \left(\frac{2}{\pi}\right) \chi_{333}^{(2)}$ (see subsection 2.4.1), which will be needed later on. As explained in subsection 3.2.2 in more detail this model also takes the effects of Gaussian optics into account.
A closer look at this model concerning energy conservation tells that this approximation breaks down for high fundamental power because the power that is converted into green light must not exceed the power that was actually sent into the crystal.
The approximation made in this model assumes a constant fundamental power all over the crystal, which is just fulfilled when conversion is low and the created harmonic power $P_2$ is much smaller than the fundamental pump power $P_1$, so that the effect, that power which is converted into harmonic light reduces the fundamental power, can be neglected.
When the generated harmonic power cannot be neglected in comparison to the fundamental power anymore a better approximation for the conversion can be achieved, if this pump depletion of the fundamental light is taken into account. For the generated harmonic power as the product of photon-flux

density (see subsection 2.2.2) and the corresponding photon energy, we then get:

$$P_2 = 2\pi\hbar\nu_2\Phi_2(z) =$$
$$2\pi\hbar 2\nu_1\frac{1}{2}\Phi_1(0)\tanh^2\left(\frac{\gamma L}{2}\right) =$$
$$P_1\tanh^2\left(\underbrace{\sqrt{\frac{8\pi\varepsilon_0^2\eta_0^3\nu_1^2}{n_2 n_1^2}\frac{P_1}{\langle\omega^2\rangle}\left((2/\pi)\,\chi^{(2)}_{333}\right)^2}}_{\gamma}\frac{L}{2}\right) = \kappa(P_1)LP_1^2 \tag{3.7}$$
$$\kappa(P_1) = \frac{\tanh^2\left(\frac{\gamma L}{2}\right)}{LP_1}$$

Note that the results in subsection 2.2.2 were originally derived for the case of perfect phase matching and that it is used here to describe the generated harmonic power for the PPLN-crystal with the nonlinear susceptibility coefficient $\chi^{(2)}_{eff} = \left(\frac{2}{\pi}\right)\chi^{(2)}_{333}$ for reasons that were already explained above.
It is easily verified that the low conversion approximation is included in this new approximation as the limit for small conversion, that means for small arguments of the *tanh*-function.
In the last line formula 3.7 was written as a function of the squared fundamental input power following the definition of the conversion efficiency in equation 3.6. Thereby all effects of pump depletion are absorbed in the conversion efficiency, which then becomes dependent on the fundamental input power and assures that not more than the initial fundamental pump power is converted into green light. The low and the high conversion approximation both are plotted in figure 3.19 together with the measurement results.

We notice that for a fundamental pump power of 6W and a corresponding green power of 0.6W the low conversion approximation already differs by about 10% relative to the measured value. There the ratio between green power and fundamental input power is $P_2/P_1 \approx 0.6\text{W}/6\text{W} = 10\%$.
The high conversion approximation predicts the measurement results quite well within the error bars for fundamental powers up to about 8.5W. For

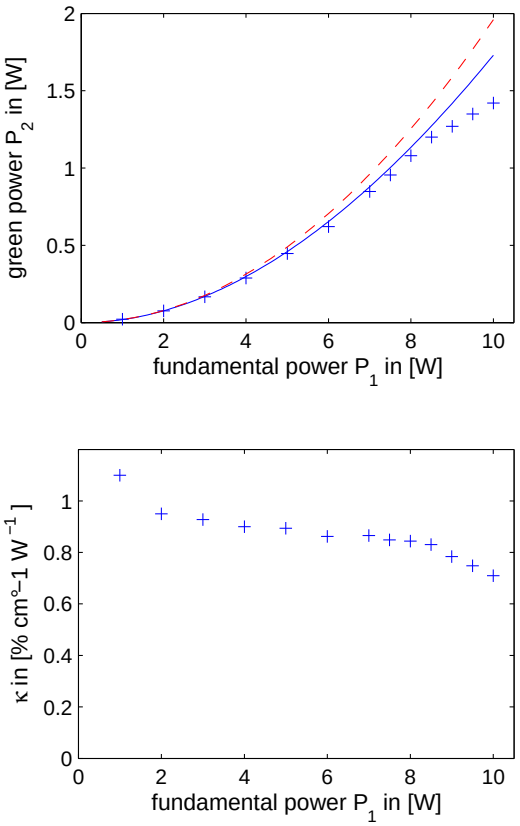


Figure 3.19: *Top*: Dependence of the converted output power $P_2$ on the fundamental input power $P_1$. The temperature of the crystal is set to its optimum temperature for each fundamental input power and a focusing to a waist $\omega_0 = 30\mu$m is used. The created harmonic power increases with increasing fundamental power and reaches a value of about 1.4W at a fundamental input power of 10W. The solid line shows a theoretical curve including pump depletion calculated by the high-conversion-approximation. The deviation of the experimental results for fundamental input powers higher than about 8.5W may be assigned to GRIIRA. For low fundamental input power below 6W pump depletion can be neglected and the low-conversion-approximation gives a good estimation of the converted output power (dashed line). *Bottom*: The conversion efficiency (definition see equation 3.6) decreases for increasing fundamental power. For a fundamental power of 10W a conversion efficiency of $0.007\mathrm{W}^{-1}\mathrm{cm}^{-1}$ is determined, that are 70% of the value for the conversion efficiency at fundamental input power of 1W. (+) represent calculated values of $\kappa$ from measurement results of $P_2$ and $P_1$.

higher fundamental powers the measured harmonic power is even lower than the high conversion model predicts. At a fundamental pump power of 10W the measured harmonic power reaches just about 1.4W, that is just about 80% of the value expected by the high-conversion model.
This decrease of harmonic light can be explained by the appearance of GRIIRA. In addition to the absorption of green light the fundamental power decreases and thus less harmonic light is generated. As GRIIRA depends on the power of green light, which increases along the crystal, it is also possible that a temperature gradient builds up. This could cause the local crystal temperature to differ from the QPM-temperature what would lead to a worse conversion.
For optimal focusing to a waist $\omega_0 = 30\mu$m and a fundamental pump power of 10W the lower limit given by Stratophase for the damage threshold of the crystal (0.5MW/cm$^2$ or higher) is exceeded. In subsection 3.2.2 we calculated an average intensity of 0.2MW/cm$^2$ and a peak intensity at the waist of ca. 0.7MW/cm$^2$.
Therefore this focusing at the fundamental power of 10W first was tested at a crystal site far off any grating by slowly ramping up the power and keep it focused into the crystal for several minutes. As no damage occurred, the fundamental light was focused into the grating, again first the grating was adjusted for optimal conversion at a low fundamental power (about 100mW) and then the power was ramped up slowly.
As explained in section 3.2.3, due to the dependence of the optimum temperature on the fundamental power, for the measurement in figure 3.19 it was necessary to adjust the temperature for each fundamental power.
For 10W of fundamental input light a green output power of 1.4W has been achieved, from which an effective conversion efficiency of $\kappa = 0.7\%\mathrm{W}^{-1}\mathrm{cm}^{-1}$ is calulated. We also watched the long term stability at this power level for several hours (see figure 3.20).

To summarize this subsection, we notice that whereas Stratophase gave a conversion efficiency of $1\%\mathrm{W}^{-1}\mathrm{cm}^{-1}$ at low fundamental power and thus a converted power of 2W should be expected when using a fundamental power

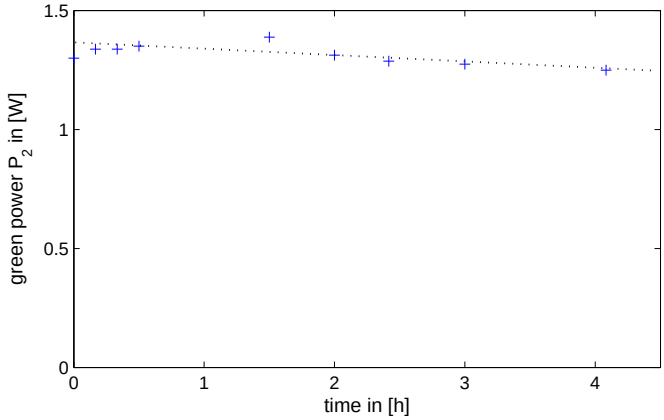


Figure 3.20: The long term stability at a green power level of 1.4W and a fundamental input power of 10W shows a nearly linear decrease with a rate of about $2\%/h$ of the green power. A main reason for this could be a drift of the fundamental power but most likely this decrease is due to the drift of the crystal's temperature. A deviation of about 0.2°C - that is already the accuracy with which the controller temperature can be set - from the optimal QPM-temperature would cause about 10% less conversion. When the fiber-amplifier runs at a high fundamental output power such as 10W it is better to stop any mechanical working in the vicinity of the fiber-amplifier because any shaking (for example when putting some optics on the optical table) causes the controller box of the fiber-amplifier to switch the amplifier off (see subsection 3.1.2).

of 10W, it turned out that we must take pump depletion into account and thus obtain some lower harmonic output power.

At high power levels of harmonic light GRIIRA decreases conversion and limits the generated power at about 1.4W. But neverheless this power seems to be high enough for our further purpose.

# Chapter 4

# Towards the 1D optical superlattice

## 4.1 Preparation of the lattice beams

The 1D optical superlattice will consist of a 3D optical lattice made by three retro-reflected beams at a wavelength of 1064nm and an additional 1D optical lattice at a wavelength of 532nm in one dimension. Thus the light that leaves the SHG apparatus must be divided up into three beams at 1064nm and one beam at 532nm. Furthermore, the power of each of the four beams must be stabilized-which will be accomplished by AOMs - and each beam must be coupled into a fiber to deliver the light to the experimental table.
For designing the setup it is important to recognize, that at the one hand the optical setup should be as compact as possible - because of stability reasons - and that there should be used as few optical elements as necessary - because of reflection losses - but on the other hand the setup should be large enough and should have a sufficient number of degrees of freedom to allow a quick and uncomplicated (re)adjustment.
Some details of the setup are explained in the following:
The separation of the fundamental IR-light and the harmonic green light is already done by the dielectric mirror. In the setup the collimating lens after the oven is adjusted in the way that it prepares a slightly convergent

fundamental beam. Thus the beam diameters at the three AOMs slightly differ in the range of about 1400$\mu$m to 1100$\mu$m and it is not necessary to use individual lenses in front of each AOM.
The fundamental beam power is divided up by four thin-film-polarizers with a low order ($\lambda/2$)-waveplate in front of each. These thin-film-polarizers offered by Linos have a extinction ratio better than 10000:1 at the transmission port for wavelength between 750nm and 1100nm, can be used for intensities up to about 1kW/cm$^2$ and are designed in the way that the angle between reflected and transmitted beam is 90°. The first cube is used to adjust the overall power and the second, third and fourth cube are used to set the proportions for sharing out this power between the three lattice beams. The two mirrors in front of each AOM are used to adjust the beams right through the AOMs by *beamwalking*.

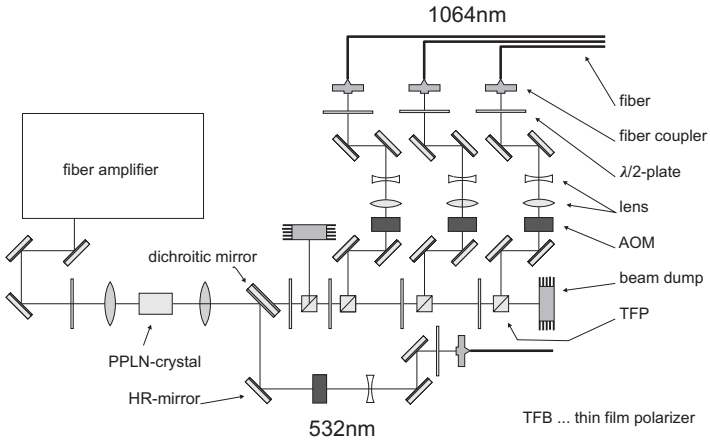


Figure 4.1: Setup of the beam-splitting-arrangement. The rest of the fundamental power, that is not converted, is divided up into three beams for the 3D optical lattice. The powers of the fundamental beams and the harmonic beam are stabilized by AOMs and coupled into fibers.

For the wavelength of 1064nm AOMs from crystal technology (Model# 3110-197) with a saturation RF-power of 2.5W at a RF-frequency of ca. 110MHz are used. A measured diffraction efficiency into the first order of 90% for the present setup was reached.
After each AOM two lenses are used as a telescope configuration to prepare

the necessary beam diameter of 1800$\mu$m$\pm$200$\mu$m for coupling into the fiber. For the fundamental wavelength of 1064nm and an optical power of 2W self-made patch cords are used ( fiber data: Nufern, HP980 cutoff wavelength 900nm, singlemode and polarization maintaining, angle-polished-fc finishes) and a coupling efficiency of 75% is reached. The polarization of the light coupled into the fiber is adjusted for minimum fluctuation of the output polarization with a ($\lambda$/2)-waveplate.
For the harmonic green beam an additional lens is used to prepare a slightly convergent beam with a beam diameter of about 800$\mu$m at the position of the AOM. For this wavelength an AOM from crystal technology (Model#3080-120) is used with a RF-saturation-power of 0.5W at a RF-frequency of 80MHz and a measured diffraction efficiency of 85% into the first order.
Before coupling into the fiber the beam is prepared to a diameter of about 1600$\mu$m. Like before a ($\lambda$/2)-waveplate is used to optimize the polarization to minimum fluctuation of the polarization at the output.
For the green light at a wavelength of 532nm and a power over 1W a high-power-patch-cord made by Ozoptics was bought. The fiber is singlemode polarization maintaining and has a cut off wavelength of 470nm. The high-power-connector at the in-coupling-side of the fiber prevents the fiberend to be burned when high powers are used.
For the out-coupling-side no such high-power-connector is necessary and therefore it is a *simple* fc-connector (with angle polished finish). We reached a coupling efficiency of about 80% into the fiber.

## 4.2 Stability of the superlattice

In this subsection some considerations and estimations concerning the necessary requirements of the setup for the 1D optical superlattice will be discussed.
The 1D optical superlattice will consist of a 3D optical lattice with wavelength $\lambda_1$ and an additional standing wave with a wavelength of $\lambda_2 = 1/2\lambda_1$ in one of the three directions. A schematic drawing of the setup is shown in figure 4.3. The setup of the overlaid lattice beams will in principle be imple-

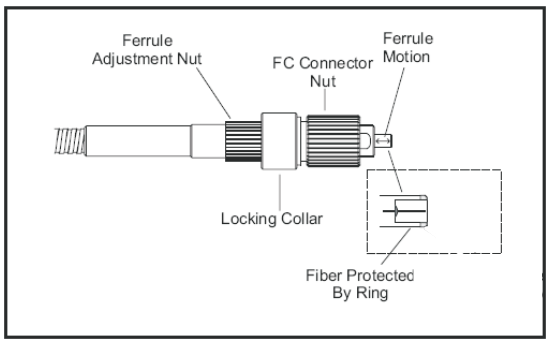


Figure 4.2: In standard connectors fibers are glued into place, and the fiber is polished flush with the connector surface. When used with high power lasers, heat generated at the tip of the fiber causes the surrounding epoxy to break down and give off gases. These gases in turn burn onto the tip of the fiber, causing catastrophic damage to the fiber. In contrast the high power connectors of Ozoptics feature an air-gap design, where the fiber extends into free space by 1.1mm to 1.5mm, providing an epoxy-free region where thermal energy is safely dissipated without burning the surrounding material (see [36]).

mented as follows: One fundamental beam ($\lambda_1 = 1064$nm) and the harmonic beam ($\lambda_2 = 532$nm) emitted from the corresponding fibers, that transport the light from the SHG-apparatus to the experimental table, are combined by a dichroitic mirror. The imaging light with a wavelength of about 780nm, resonant to the $D_2$-line of $^{87}$Rb ($F=2 \rightarrow F'=3$), is overlaid to these two lattice beams by a thin-film-polarizer. The polarizations of the waves are chosen in the way that fundamental and harmonic light are reflected by the thin-film-polarizer while the imaging light is transmitted. These three beams then propagate along the same direction into the glass cell through the atomic cloud. After the glass cell first the imaging light is separated from the lattice light by a thin-film-polarizer and then the lattice light is split into the fundamental and harmonic component by a dichroitic mirror. Each of the two beams is then retro-reflected by a mirror and thus builds up a standing wave. To shift the two standing waves relative to each other and to stabilize this relative phase, one of the retro-reflecting mirrors is glued onto a piezoelectric

actuator.

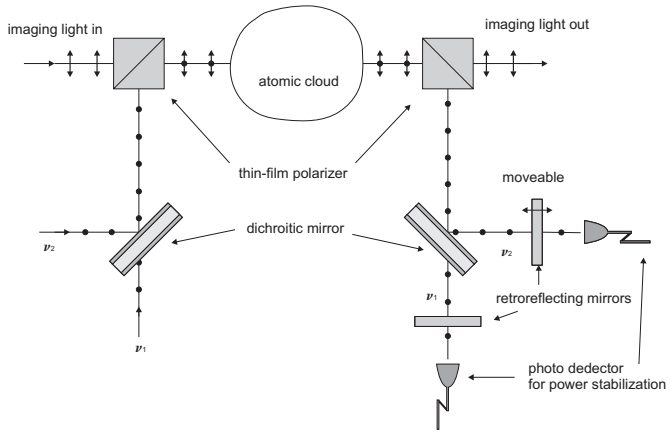


Figure 4.3: Possible setup for the superlattice. The fundamental and harmonic wave are overlaid and separated again by dichroitic mirrors. To adjust the relative phase between the two standing waves one retro-reflecting morror can be moved by a piezo. (Not shown are the beams in the other two directions of space.)

The photo-diodes behind the retro-reflecting mirrors supply the signal for stabilization of the corresponding power of the fundamental and harmonic light. As already mentioned in section 4.1 the power stabilization will be done by the AOMs, which are put in front of each fiber (see figure 4.1).
The light field of the involved lattice beams causes a periodic lattice potential for the ultracold atomic gas. For $^{87}$Rb atoms the fundamental standing wave causes an attractive potential while the harmonic standing wave causes a repulsive potential. By combining both standing waves it is possible to modify the potential felt by the atoms. For example by suitable changing of the relative phase between the two standing waves and the intensitys of the two waves it is possible to construct a lattice of double-well potentials with arbitrary energy shifts $\Delta E$ of the two minimas and adjustable barrier height $E_b$ inbetween the two wells (see figure 4.4). The ability to control the potential shape by the relative phase between the two standing waves makes the system also sensitive to relative phase fluctuations due to ambient perturbations. Such unwanted phase fluctuations could arise from jittering of

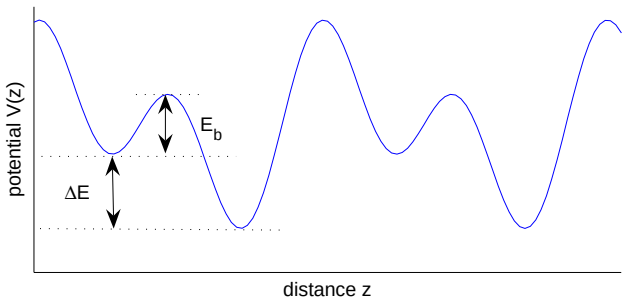


Figure 4.4: By combining two standing waves with $\lambda_1 = 2\lambda_2$ it is possible to generate a periodic double-well potential. The energy difference $\Delta E$ and the barrier height $E_b$ between neighbouring wells can be varied by changing the relative phase between the two standing waves and their intensities.

the different lattice mirrors relative to each other and from dispersion in air. Imperfections of the stability of the two wavelengths relative to each other can affect the periodicity of the double-well lattice. So to guarantee a stable shape of a periodic lattice potential at the location of the atomic cloud it is necessary to stabilize the two frequencies relative to each other and to keep the relative phase between the fundamental and the harmonic standing wave as stable as possible. In the following the perturbations mentioned above are discussed in more detail.

To achieve a periodic double-well potential with sufficient good periodicity, the wavelengths of two lattice beams - with $\lambda_1 \approx 2\lambda_2$ - must be frequency locked. In our experiment we accomplish this by SHG and we use the fundamental and the harmonic light to produce the necessary lattice beams.

There is quite some distance between the retro-reflecting mirrors and the atomic cloud, so that the beams propagate quite some distance in air. As the actual superlattice consists of two standing waves with different wavelengths and as the relative phase between these standing waves at the position of the atomic cloud affects the potential shape decisively (see figure 4.4), the dispersion of air must be taken into account.

The dispersion between the fundamental and harmonic wave depends on the air-temperature and the air-pressure. Fluctuations of these two parameters

thus cause fluctuations of the relative phase. Therefore to achieve a potential with sufficient stable shape, results in restrictions for the stability of air-temperature $\Delta T$ and air-pressure $\Delta p$. For a quantitative statement on this, we assume an optical way with a length $l$ and a phase difference stability $\Delta\phi$, that is wished to be achieved, and estimate the necessary stability $\Delta T$ and $\Delta p$ of the temperature and the pressure of the surrounding air:
Therefore the relative phase $\phi$ between the fundamental and harmonic standing wave due to dispersion in air is defined as the difference of the phase of a harmonic wave with the real refractive index $n_2$ and the phase of a fictitious harmonic wave with the refractive index $n_1$ corresponding to the real refractive index of the fundamental wave in air. Thus the phase difference is calculated as:

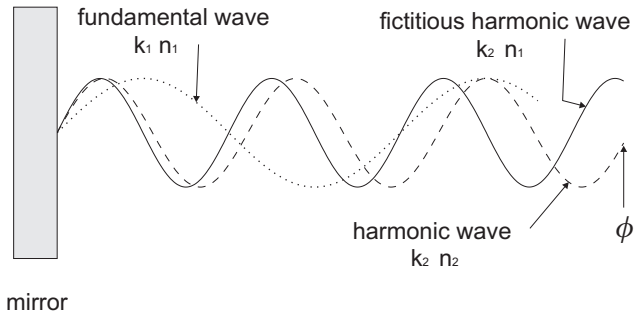


$$\phi = k_2 l\,(n_2 - n_1) =$$
$$\frac{2\pi}{\lambda_2} l\,(n_2 - n_1) = \frac{2\pi l}{\lambda_2}\left((n_2 - 1)_{pT} - (n_1 - 1)_{pT}\right) \tag{4.1}$$

Where $k_2 = 2\pi/\lambda_2$, $\lambda_2$ is the wavelength of the harmonic beam and $n_1$ and $n_2$ are the corresponding refractive indices for a fundamental and harmonic wave propagating in air. The last line was written in a form, so that the following equations 4.2 and 4.3 can easily be applied. The two indices $T$ $p$ just denote the dependences on temperature and pressure.
The dependence of the refractive index in air on the temperature T and the pressure $p$ is given by [37]:

$$(n-1)_{pT} = (n-1)_s 0.00138823 \times \frac{p/\text{torr}}{1 + 0.003671 T/^\circ\text{C}} \tag{4.2}$$

In this formula temperature is given in °C and pressure is given in *torr*. Where $(n-1)_S$ denote the standard values of the refractive index, which correspond to the temperature of 15°C and the pressure of 760torr(1064mbar). These standard values for light with a wavelength $\lambda$ in $\mu$m are given by [37]:

$$(n-1)_s \times 10^8 = 8342.13 + 2406030(130 - (\lambda/\mu\text{m})^{-2})^{-1} + 15997(38.9 - (\lambda/\mu\text{m})^{-2})^{-1} \tag{4.3}$$

For the following calculations will also be used, that the surrounding air in the laboratory has a temperature of about 25°C and a pressure of about 950mbar (710 torr).
With this the fluctuation $\Delta\phi$ of the relative phase due to fluctuations $\Delta T$ of the air-temperature and $\Delta p$ of the air-pressure can be estimated by writing equation 4.1 in differential form and evaluating the necessary partial derivatives by use of equations 4.2 and 4.3 as:

$$\Delta_T\phi := \frac{\partial\phi}{\partial T}\Delta T = \frac{2\pi l}{\lambda_2}\left(\frac{\partial(n_2-1)_{pT}}{\partial T} - \frac{\partial(n_1-1)_{pT}}{\partial T}\right)\Delta T \approx -1.2\frac{2\pi l}{\lambda_2}10^{-8}\Delta T/°\text{C}$$

$$\Delta_p\phi := \frac{\partial\phi}{\partial p}\Delta p = \frac{2\pi l}{\lambda_2}\left(\frac{\partial(n_2-1)_{pT}}{\partial p} - \frac{\partial(n_1-1)_{pT}}{\partial p}\right)\Delta p \approx 0.5\frac{2\pi l}{\lambda_2}10^{-8}\Delta p/\text{torr}$$

When a stability of the relative phase between fundamental and harmonic standing wave of $\Delta\phi = 0.1\pi$ should be achieved for an optical way in air of about $l = 1$m and with $\lambda_2 = 532$nm the allowed fluctuations $\Delta T$ of the surrounding temperature and $\Delta p$ of the surrounding pressure are thus estimated as:

$$\Delta T \leq \frac{\Delta\phi}{1.2}\frac{\lambda_2}{2\pi l}10^8\ °\text{C} \approx 2\ °\text{C}$$

$$\Delta p \leq \frac{\Delta\phi}{0.5}\frac{\lambda_2}{2\pi l}10^8\ \text{torr} \approx 5\ \text{torr}$$

In the setup shown in figure 4.3 the fundamental and harmonic wave are separated by a dichroitic mirror and propagate along different ways before they are retro-reflected and compined again. Different fluctuations of the temperature or the pressure along the two different ways as well as mechanical vibrations of the two retro-reflecting mirrors relative to each other

can affect the relative phase between the two standing waves and thus the potential shape at the position at the atomic cloud. With a Michelson interferometer configuration the stability for a setup shown in figure 4.3 was tested. The observed fluctuation of the relative phase of the Michelson interferometer configuration is expected to give an estimation for the order of magnitude of the fluctuation in the real setup. In the interferometer configuration one retro-reflecting mirror was fixed at a distance of about 2cm to the beamsplitter the second retro-reflecting mirror was fixed at different distances, to check if the fluctuations depend on the size of the setup. For each configuration the interference signal was observed with a photo-detector. The results in figure 4.5 show that a relative phase stability of about $0.1\pi$ for several minutes without any regulation is achieved by choosing a compact setup. The time scale for typical fluctuations is about $\tau > 5$s.

In summary the calculations and measurements show that the smaller the setup is build the smaller are the fluctuations due to the separation of the two waves and due to fluctuations of the surrounding air-temperature and air-pressure. Thus on the one hand the setup should be as compact as possible to guarantee sufficient stability of the lattice-potential but on the other hand the setup should be large enough to allow a good handling of all the necessary optical elements. Whether this stability of the relative phase is sufficient and how stable the whole system has to be, must be tested by real experiments with the atomic cloud, which was not done so far during this work.

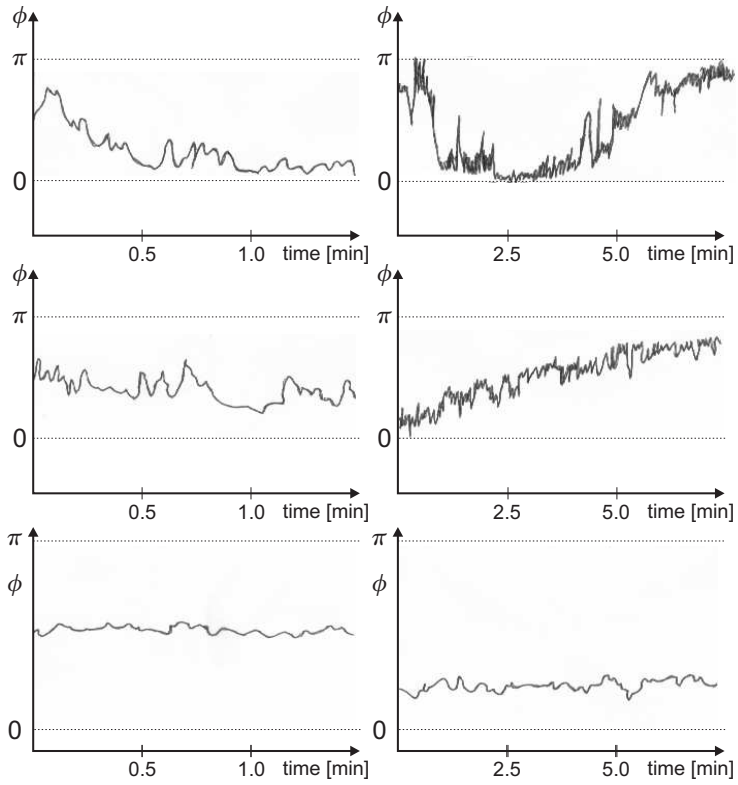


Figure 4.5: Shown is the behaviour of the fluctuations of the relative phase $\phi$ of a Michelson interferometer configuration. For each measurement one retro-reflecting mirror is fixed close to the beam splitter at a distance of about 2cm and the second retro-reflecting mirror is fixed at different distances (*top* 20cm, *middle* 10cm, *bottom* 2cm). The corresponding interference signals and thus the fluctuations of $\phi$ are shown in the diagrams. The observation time is 1.5min for the diagrams on the left and 7.7min for the diagrams on the right. These measurement results show that the smaller the setup is implemented the lower the fluctuation of the relative phase gets. For a compact setup (bottom diagrams) with both retro-reflecting mirrors in a distance of about 2cm from the beamsplitter the relative phase fluctuates slowly with a timescale $\tau > 5$s within about $0.1\pi$ for several minutes.

# Chapter 5

# Summary and Outlook

In this thesis the setup of a single pass second-harmonic generation (SHG) apparatus with PPLN as the nonlinear medium was described. In periodic modulated nonlinear media like periodically poled lithium niobate (PPLN) second-harmonic generation is achieved by Quasi-Phase Matching (QPM).
In future experiments, the fundamental and the harmonic light will be used to implement a 1D optical superlattice. In our case the optical superlattice is a periodic double-well potential for $^{87}$Rb-atoms. To achieve sufficient high conversion of fundamental light into harmonic light the whole SHG-arrangement had to be optimized, which represents the main content of this thesis.
I found the following results:
It is important that the fundamental light is well polarized, because effectively just the component of the fundamental light parallel to the optical axis of the crystal is converted. The PPLN-crystal is designed to work for this polarization because then the highest possible component of the nonlinear susceptibility for lithium niobate can be used.
I also found that there exists an optimum waist for focusing the fundamental light into the crystal. In principle, for a high conversion the averaged intensity of fundamental light along the whole crystal must be as high as possible. Hence, Gaussian optics must be taken into account. To obtain a rough estimation of the optimum waist, a good rule of thumb is to choose

the waist, which belongs to a Gaussian beam with a Rayleigh length that equals half the crystal length. It turns out, that for the present crystal the experimentally determined optimum waist of 30$\mu$m is somewhat smaller than the value obtained from the previous estimation. Regarding this, a model for calculating the dependence of the conversion on focusing of the fundamental light was developed which agrees quite well with the experimental measurement results. For efficient SHG with our crystal it was found, that for optimum focusing it is also necessary to adjust the position of the focus inside the crystal along the direction of propagation with an accuracy in the mm-range.

The fine tuning for QPM of the fundamental and the harmonic light is achieved by tuning the crystal temperature. The actual optimum temperature depends on the poling period of the chosen grating on the PPLN-crystal. For stable conversion this optimum temperature must be kept with an accuracy better than 0.1°C. Because of disturbing heating effects due to absorption of harmonic and fundamental light and the limited temperature control of the crystal, the set value of the PID-controller for the optimum temperature must be decreased with increasing fundamental power.

We also investigated the dependence of conversion on the fundamental input power. In the case of high conversion pump depletion must be taken into account, because the creation of one harmonic photon consumes two photons of fundamental light. Further, the conversion is decreased by the appearance of Green-Induced-InfraRed Absorption (GRIIRA), so that we end up with a generated harmonic power of about 1.4W for SHG with fundamental light with a power of about 10W.

By using SHG for the production of the lattice beams the two different frequencies are already intrinsically frequency locked, which is necessary for a stable periodic double-well potential. I also made further considerations and estimations about the stability of the optical superlattice concerning the necessary stability of the relative phase between the two standing waves, which make up the superlattice. For the implementation of the superlattice shown in figure 1.1 on page 7 relevant fluctuations of the relative phase due

to fluctuations of air-temperature[1] and air-pressure are expected to be slow compared to the typical time scale for a single experimental cycle. These fluctuations together with the fluctuations arising from vibrations of the two retro-reflecting mirrors relative to each other can be minimized when a compact setup for the relevant parts is chosen. Nevertheless long term drifts of temperature and pressure could cause trouble with the desirable repeatability of subsequent measurements. Whether the so implemented superlattice is stable enough must still be tested in experiments with the ultracold atoms.

Controllable double-well lattices offer new possibilities for manipulating individual atoms. As shown in [17] atoms can be transported coherently and also coherent splitting of atoms has already been demonstrated in [11, 17]. Various quantum gate proposals with neutral atoms relaying on controllable double-well potentials have already been developed. The high potential of optical lattices for quantum computation has already been shown in [17, 13, 18, 19, 20, 7]. In the following, one of those will be explained in more detail.
The QIP-scheme proposed in [7], which we want to impement in the future, is based on a concept using so called register and marker atoms and involves the transport of atoms by a spin-independent controllable double-well lattice. Starting point of this scheme is a regular array of micro traps realized by optical lattices. The qubits are stored separately - one in every lattice site - so that they never interact directly with each other. A high number of qubits in such an array is essential for fault-tolerant quantum computation. The advantage for using spin-independent optical lattices is that decoherence due to spontaneous emission is suppressed because for the lattice beams far-off resonant light can be used. Further, for spin-independent lattices the internal atomic state can be freely chosen, so that it is possible to use an atomic state, which is insensitive to (stray) magnetic fields - thus again improving decoherence.

[1]The relevant parts for fluctuations of the relative phase are the distances between the glass cell and the retro-reflecting mirrors. Along these paths the corresponding waves propagate in air, which is a dispersive medium.

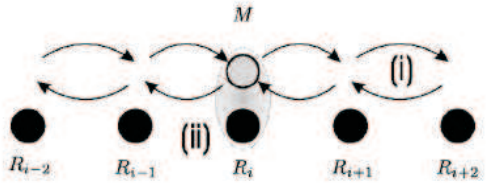


Figure 5.1: Basic operation with a marker atom M on a quantum register $R_i$: (i) forward and backward transport steps, (ii) local interaction with register qubits. (Picture taken from [7].)

While the register atoms are frozen at their specific lattice site, marker atoms are moved forward and backward between different lattice sites through the array of register-atoms in a controlled way (see figure 5.1). The controlled transport of the marker atoms is achieved by globally changing the external lattice control parameters. These control parameters are the intensities and the relative position of the two standing waves, that make up the double-well potential. By changing these external control parameters properly, several marker atoms even if prepared in a certain spatial pattern will be moved in parallel.

The marker atoms fulfill two purposes. Marker atoms selectively address single qubits and they also act as a messenger for transporting quantum information between two distant register qubits. Moving the marker atom to a specific site of a register atom allows to address exactly this atomic qubit due to the marker atomic qubit interaction. Thus atomic qubits can be selectively manipulated with a laser without the requirement of focusing the laser on a particular site. The transport of quantum information between different sites can be used to entangle distant atomic qubits ( see figure 5.2).

Single and two qubit gate operations can be performed by employing resonant molecular interactions between marker and qubit atom provided by magnetic or optical feshbach resonances as described in [7].

In sum the proposal [7] relies on techniques that are presently being developed, and represents therefore a feasible candidate for the implementation of QIP with neutral atoms in optical lattices.

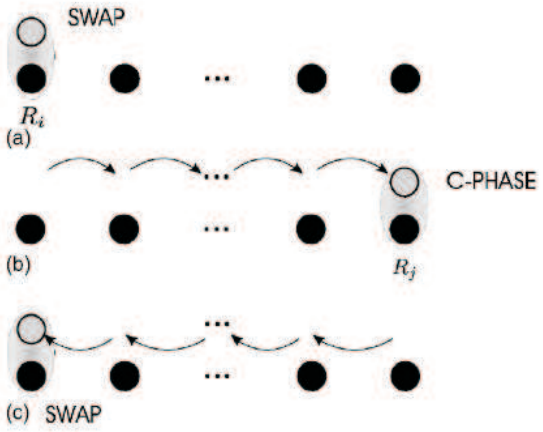


Figure 5.2: Realizing an entangeling operation between distant atoms based on the elementary steps described in figure 5.1: (a) swapping the first qubit onto the marker atom, (b) transporting the marker atom unto the second qubit and local interaction, (c) transport back to the first qubit and inverse swap. (Picture taken from [7].)

Optical lattices and dynamic controllable double-well potentials offer new opportunities also for other applications. Beside the simulation of models in solid state physics like [5, 6], these periodic potentials can be used for tunneling experiments like [9], for the investigation of entanglement of atoms due to controlled collisions between the atoms [12, 13] and for the study of repulsively bound objects [21].
Thus pushing further the research of ultracold atoms in controllable optical lattices will offer the ability for implementing many proposals and will bring many new insights not only for fundamental concepts of quantum mechanics but also for new applications.

***Useful constants and frequently used variables:***

| | | |
|---|---|---|
| $\varepsilon_0$ | $8.8542 \times 10^{-12}$F/m | Permittivity of free space |
| $\mu_0$ | $1.2566 \times 10^{-6}$H/m | Permeability of free space |
| $\eta_0 = \sqrt{\mu_0/\varepsilon_0}$ | $377\Omega$ | Impedance of free space |
| $h = 2\pi\hbar$ | $6.6262 \times 10^{-34}$J s | Planck's constant |

| | |
|---|---|
| $n_q$ | Refractive index of wave q |
| $q = 1$ | denotes the fundamental wave |
| $q = 2$ | denotes the harmonic wave |
| $\Delta n = \lvert n_2 - n_1 \rvert$ | Difference of the refractive indices |
| $\chi$ | Linear electric susceptibility tensor |
| $\chi^{(2)}$ | Nonlin. $2^{nd}$ order electr. suscept. tensor [m/V] |
| $\mathscr{P}$ | Electric polarization density |
| $L$ | Length of the crystal |
| $\mathscr{E}$ | Electric field [V/m] |
| $E_q$ | Electric-field complex amplitude [V/m] |
| $\nu_q$ | Frequency of wave q [Hz] |
| $\lambda_q$ | Wavelength of wave q |
| $k_q$ | Wavevector of wave q |
| $\Delta k = \lvert k_2 - 2k_1 \rvert$ | Deviation from the phase-matching condition |
| $I_q$ | Intensity of wave q |
| $\Phi_q = \lvert a_q \rvert^2$ | Photon-flux density of wave q [$m^{-2}$ $s^{-1}$] |
| $S$ | Poynting vector |
| $\omega$ | Beam radius |
| $\omega_0$ | Beam waist |
| $z_0$ | Rayleigh length |
| $g$ | Coupling coefficient see page 14 |
| $\gamma$ | Gain coefficient see page 18 |
| $l_c$ | Coherence length |
| $P_q$ | Power of wave q |
| $\kappa$ | conversion efficiency [$W^{-1}$ $cm^{-1}$] |

# Bibliography


[1] O. Morsch, J.H. Müller, M. Christiani, D. Ciampini, and E. Arimondo, Phys. Rev. Lett. **87**, 140402 (2001).

[2] M. Greiner et al., Nature **415**, 39 (2002).

[3] D. Jaksch et al., Phys. Rev. Lett. **81**, 3108 (1998).

[4] G. Thalhammer, K. Winkler, F. Lang, S. Schmid, R. Grimm, and J. Hecker Denschlag Phys. Rev. Lett. **96**, 050402 (2006).

[5] A.M. Rey, V. Gritsev, I. Bloch, E. Demler and M.D. Lukin, arXiv: 0704.1413

[6] B.Paredes, C. Tejedor, and J.I. Cirac, Phys. Rev. A **71**, 063608 (2005).

[7] T. Calarco, U. Dorner, P.S. Julienne, C.J. Williams, and P. Zoller, Phys. Rev. A **70**, 012306 (2004).

[8] A. Görlitz, T. Kinoshita, T.W. Hänsch, and A. Hemmerich, Phys. Rev. A **64** (2001).

[9] S. Fölling, S. Trotzky, P. Cheinet, M. Feld, R. Saers, A. Widera, T. Müller and I. Bloch, Nature **448** (2007).

[10] P.J. Lee, M. Anderlini, B.L. Brown, J. Sebby-Strabley, W.D. Phillips, and J.V. Porto, Phys. Rev. Lett. **99**, 020402 (2007).

[11] J. Sebby-Strabley, M. Anderlini, P.S. Jessen, and J.V. Porto, arXiv:cond-mat/0602103 (2006).

[12] A. Widera, O. Mandel, M. Greiner, S. Kreim, T.W. Hänsch, and I. Bloch, Phys. Rev. Lett. **92**, 16 (2004).

[13] O. Mandel, M. Greiner, A. Widera, T. Rom, T.W. Hänsch and I.Bloch, letters to nature **425** (2003).

[14] M. Greiner, I. Bloch, T.W. Hänsch und T. Esslinger, Phys. Rev. A **63** (2001).

[15] T. Esslinger, I. Bloch und T.W. Hänsch, Phys. Rev. A **58** (1998).

[16] M. Theis, Optical Feshbach Resonances in a Bose-Einstein Condensate, PhD thesis, Universität Innsbruck (2005).

[17] O. Mandel, M. Greiner, A. Widera, T. Rom, T.W. Hänsch and I.Bloch, Phys. Rev. Lett. **91**, 1 (2003).

[18] S. Peil, J.V. Porto, B. Laburthe Tolra, J.M. Obrecht, B.E. King, M. Subbotin, S.L. Rolston, and W.D. Phillips, Phys. Rev. A **67** (2003).

[19] B. Laburthe Tolra, et al., Phys. Rev. Lett. **92**, 190401 (2004).

[20] H. Moritz et al., Phys. Rev. Lett. **91**, 250402 (2003).

[21] K. Winkler, G. Thalhammer, F. Lang, R. Grimm, J. Hecker Denschlag, A. J. Daley, A. Kantian, H. P. Buechler, P. Zoller, Nature **441**, 853 (2006).

[22] B.E.A. Saleh, M.C. Teich, "Fundamentals of Photonics", Wiley, New York, 1991.

[23] G.A. Reider, "Photonik", Springer, Wien, 1997.

[24] K. Stierstadt, "Physik der Materie", VCH, New York, 1998.

[25] C. Kittel, "Einführung in die Festkörperphysik", Oldenbourg, München, 2002.

[26] G.D. Miller, R.G. Batchko, W.M. Tulloch, D.R. Weise, M.M. Fejer, R.L. Byer, "42% efficient single-pass cw second harmonic generation in periodically poled lithium niobate", Opt. Lett. **22**, 1834 (1997).

[27] Properties of Lithium Niobate, EMIS Data Reviews Series No.**5** (INSPEC, London, 1989).

[28] R.S. Weis and T.K. Gaylord, "Lithium Niobate: Summary of Physical Properties and Crystal Structure," Applied Physics A **37** (1985)pp. 191-203.

[29] A. Rauber, "Chemistry and Physics of Lithium Niobate," in Current Topics in Materials Science, vol. **1**, Ed E. Kaldis (North-Holland, Amsterdam, 1978) pp. 481-601.

[30] Landolt-Bornstein,"Numerical data and functional relationships in science and technology," New Series, vol. III/16 and III/28a.

[31] A. Ashkin, G.D. Boyd, J.M. Dziedzic, R.G. Smith, A.A. Ballmann, J.J. Levinstein, K. Nassau: Appl. Phys. Lett. **9**, 72 (1966).

[32] F.S. Chen, J.T. LaMaccia, D.B. Fraser: Appl. Phys. Lett. **13**, 223 (1968).

[33] www.casix.com

[34] www.crystaltechnology.com

[35] Y. Furakawa, K. Kitamura, A. Alexandrovski, R.K. Route, M.M. Fejer, G. Foulon, "Green-induced infrared absorption in MgO doped $LiNbO_3$", Appl. Phys. Lett. **78** (2002) pp. 1970-1972.

[36] www.ozoptics.com

[37] B. Edlén, "The Refractive Index of Air", Metrologia **2**, 71 (1966).

[38] G.D. Miller, "Periodically poled lithium niobate: Modeling, fabrication and nonlinear-optical performance.", dissertation, July 1998.

[39] A. Liem, J. Limpert, H. Zellmer, and A. Tünnermann, Opt. Lett. **28** 1537 (2003).

# Danke

Dass ich bis hier hin gelangt bin, verdanke ich der Unterstützung und der Mithilfe zahlreicher anderer Personen, bei denen mich zu bedanken, ich nicht vergessen möchte:
Erster Dank gilt natülich meinem Betreuer Johannes Hecker-Denschlag für die Betreuung während meiner Diplomarbeit. Funktionierte erst mal etwas nicht so wie geplant, dann haben mich seine aufmunternden und ehrlichen Worte neu motiviert und mit seinen anschließenden Erklärungen und Anleitungen konnte ich viele Probleme doch noch bewältigen. Danke Johannes, auch für Deine Geduld vor allem mit meinem Tiroler Dialekt und dass ich immer mit Deiner Unterstützung rechnen durfte.
Auch bedanken möchte ich mich bei Rudi Grimm, nicht nur dafür, dass ich meine Diplomarbeit in seiner "ultracoolen" Forschergruppe[2] durchführen durfte, sondern auch für die hilfreichen Motivations- und Denkanstösse, die so manches beschleunigten.
Dank gebührt natürlich auch den Mitgliedern des Rb-team, die mich nett aufgenommen und mir bei den ein oder anderen experimentellen sowie prinzipiellen physikalischen Schwierigkeiten weitergeholfen haben: Danke Forian, Klaus, Gregor, Sascha, Stefan und Birgit.
Für die angenehme Atmosphäre danke ich auch meinen BürokameradInnen Francesca, Hans und Stefan, die auch öfter für meine Fragen herhalten mussten.
Sehr nützlich und hilfreich ist vor allem die sehr gute Zusammenarbeit zwischen den einzelnen Projektgruppen. Sei es für das Ausleihen von Equipment oder für die Auskunft bei technischen Angelegenheiten. Danke, dass ich mich auf Eure Hilfe und Kooperation verlassen konnte. Die Unterstützung von Elmar und Mattias habe ich diesbezüglich wohl am häufigsten beansprucht.
Danke aber nicht nur, dass man jeden von Euch immer und überall alles fragen konnte, sondern auch für die ein oder andere Kuchenrunde. -Wenn

[2]Homepage www.ultracold.at!

ich auch selten der lauteste war, habe ich diese dennoch stets genossen.
Nicht vergessen will ich auf unsere Sekretärin Christine und auf alle anderen Mitarbeiter für die große Unterstützung etwa bei administrativen oder elektro- bzw. metalltechnischen Angelegenheiten. Danke.
Die Worte des Dankes nun fast abgeschlossen, sei noch erwähnt, dass ich meine Diplomarbeit aus dem Gebiet der Quantenoptik wählte, weil mich dieses Gebiet damals interessiert hat. Jetzt, mit wieder etwas mehr Einsicht in die experimentellen Praktiken und mit wieder etwas mehr Information über die prinzipiellen physikalischen Hintergründe, muss ich zugeben, dass mich dieses Gebiet eigentlich noch viel mehr begeistert, als ich das ursprünglich angenommen habe. "Schuld" daran sind sicher der Enthusiasmus und die Begeisterung für Physik, welche die Mitglieder dieser Gruppe leben.

Sehr großer Dank gilt nicht zuletzt meiner Familie: Trotz begrenzter Mittel war die freie Wahl meines Studiums selbstverständlich, gleich wie die liebevolle und fürsorgliche Unterstützung meiner Eltern während all der Jahre. - Danke Mama und Papa[3], dass Ihr mir dies ermöglicht habt. Danke auch meinen Geschwistern Miriam, die mir stets zeigt, sich nicht unterkriegen zu lassen, und Bernhard, mit dem zusammen schier nichts nicht bewältigt werden kann. Danke auch meiner Oma, für die Unterstützung in jeglicher Art und für die Ruhe und Geborgenheit, die Du vermittelst, nicht nur wenn wir Dich zum Kiachl-essen besuchen.
Meinen Freunden und Kollegen, danke für den nötigen Ausgleich und die Abwechslung neben dem Studium: ob mit dem "runden Leder" auf dem grünen Rasen, im Kino oder beim Kartenspielen ...

[3]Trotz der leider viel zu kurzen gemeinsamen Zeit.